

This is an Open Access document downloaded from ORCA, Cardiff University's institutional repository: <https://orca.cardiff.ac.uk/id/eprint/159968/>

This is the author's version of a work that was submitted to / accepted for publication.

Citation for final published version:

Gariboldi, Karen, Pike, Jennifer , Malinverno, Elisa, Di Celma, Claudio, Gioncada, Anna and Bianucci, Giovanni 2023. Paleoceanographic Implications of Diatom Seasonal Laminations in the Upper Miocene Pisco Formation (Ica Desert, Peru) and Their Clues on the Development of the Pisco Fossil-Lagerstätte. *Paleoceanography and Paleoclimatology* 38 (5) 10.1029/2022PA004566

Publishers page: <http://dx.doi.org/10.1029/2022PA004566>

Please note:

Changes made as a result of publishing processes such as copy-editing, formatting and page numbers may not be reflected in this version. For the definitive version of this publication, please refer to the published source. You are advised to consult the publisher's version if you wish to cite this paper.

This version is being made available in accordance with publisher policies. See <http://orca.cf.ac.uk/policies.html> for usage policies. Copyright and moral rights for publications made available in ORCA are retained by the copyright holders.



1 Paleooceanographic implications of diatom seasonal laminations in the Upper Miocene
2 Pisco Formation (Ica desert, Peru) and their clues on the development of the Pisco
3 Fossil-Lagerstätte.

4

5 Karen Gariboldi¹, Jennifer Pike², Elisa Malinverno³, Claudio Di Celma⁴, Anna Gioncada¹ and
6 Giovanni Bianucci¹

7

8 ¹Dipartimento di Scienze della Terra, Università di Pisa, Pisa, Italia.

9 ² School of Earth and Environmental Sciences, Cardiff University, Cardiff, UK.

10 ³Dipartimento di Scienze dell'Ambiente e di Scienze della Terra, Università di Milano-Bicocca,
11 Milano, Italia.

12 ⁴Scuola di Scienze e Tecnologie, Università di Camerino, Camerino, Italia.

13

14 *Corresponding author:* Karen Gariboldi karen.gariboldi@unipi.it, Dipartimento di Scienze della
15 Terra, Università di Pisa, via Santa Maria 53, 56126, Pisa (Italia).

16

17 *Keywords:* mixed lamina-*Coscinodiscus* lamina duplet; permanent El Niño (El Padre); fall-dump;
18 Western and Eastern Pacific temperature gradient; biogenic silica as upwelling proxy.

19

20 *Keypoints:*

21 - Laminae of the Upper Miocene diatomaceous Pisco Formation reveal that the fall dump
22 mechanism regulated marine export production;

23 - The predominance of fall dump over upwelling implies a drop of the temperature gradient
24 between the Western and Eastern Pacific;

25 - Evidences highlight a need of caution when using biogenic silica as a proxy for paleo upwelling.

26

27 ABSTRACT

28

29 The detailed study of diatom laminations conducted by means of backscattered electron imaging
30 serves as tool to unravel details of past ocean dynamics. In this paper we apply this method to the
31 analysis of the diatomites of Cerro Los Quesos, Upper Miocene Pisco Fm, Peru. Numerous studies
32 have been conducted on the Pisco Fm; however, a focus on its paleoceanographic significance is
33 still lacking. In this work, we provide information on the oceanographic setting in the area at the
34 time of diatomites deposition. The high abundance of deep-living *Coscinodiscus* laminae,
35 proceeded by either a mixed lamina or a terrigenous one, let us hypothesize a deep position of the
36 thermocline during the deposition of the Pisco diatomites; together with the scarcity of *Chaetoceros*
37 *Hyalochaete* spp. resting spores, this evidence confutes the belief that equals high biogenic silica
38 content in marine sediments with enhanced upwelling. Conversely, the depositional setting of the
39 Pisco Fm diatomites is more similar to what is known as “permanent El Niño” (or “El Padre”) state,
40 meaning a constant weakened upwelling (or upwelling of nutrients-poor waters). Climate modeling
41 warns that an increase in atmospheric CO₂ may lead to this mean state in the near future. Thanks to
42 this study we also obtained refined information on the diatomites sedimentations rates. The
43 comparison of the Pisco diatomites sedimentation rates with those of Quaternary diatomites gave
44 strength to the hypothesis that the formation of the vertebrate Lagerstätte may have been enhanced,
45 among others, by the so-called “impact-burial” mechanism.

46

47 PLAIN LANGUAGE SUMMARY

48

49 Some sedimentary rocks are formed by the remains of small organisms. This is the case of diatoms,
50 microscopic algae with a siliceous exoskeleton. As we know the ecological conditions of the
51 modern oceans in which different diatom species live, when we found them in sedimentary rocks,

52 we can infer the ecological conditions of the oceans millions of years ago. Here, we present the
53 species that we found in some Peruvian rocks, the so-called Pisco Formation, which dates back to
54 7/6 Million of years ago. Different species are preserved in these rocks in the same order in which
55 they bloomed, so that we can identify small “laminae” (horizontal strips in the rock with thicknesses
56 smaller than 1 mm) for each blooming season. The species that we recognise are those that today
57 bloom during “El-Niño”, a climatic warm condition that causes loss of large fishery stocks,
58 inundations and droughts. This small finding helps us hypothesize how climate may evolve if the
59 Earth’s temperatures keep on rising. Also, the Pisco formation is famous because of their huge
60 content of fossil whales and dolphins, thus the study of this rock helps us understand how these
61 large mammals got preserved trough millions of years.

62 63 1. INTRODUCTION

64
65 The Late Miocene Pisco Fm, southwestern Peru, is an exceptional marine vertebrate Lagerstätte.
66 Although its vertebrate fossil content has been deeply investigated for years (Lambert et al. 2010;
67 Esperante et al., 2015; Collareta et al. 2015, 2021; Bianucci et al., 2016a and b; Gioncada et al.,
68 2016; and references therein), an interpretation of the paleoceanographic setting existing during the
69 Pisco Fm deposition is still lacking. This deficiency contrasts with the informative potential on the
70 paleoceanography of the area that these sediments hold. Indeed, part of the formation, as observed
71 at the site of at Cerro Los Quesos (CLQ, Pisco Fossil Lagerstätte Ica Desert, Peru; Fig. 1A, B), is
72 made up of laminated diatomites, of which existing literature has largely proved the potential.

73 Previous high-resolution studies of laminated diatom-rich marine sediments have provided
74 important insights into past seasonal cycles of phytoplankton productivity (Kemp et al., 2000; Pike
75 et al., 2001; Stickley et al., 2005; Davies et al., 2009; Maddison et al., 2012; Pike and Stickley,
76 2013; Davies and Kemp 2016) by comparing the sequences of laminations with modern diatom
77 seasonal assemblages obtained from sediment traps (e.g. Dunbar and Berger, 1981; Thunnel et al.,
78 1993; Sancetta, 1995) in different environments, such as upwelling areas (Peruvian forearc basins:
79 Kemp, 1990, Brodie and Kemp, 1994; Gulf of California: Pike and Kemp, 1996b, 1997, 1999;
80 Santa Barbara Basin: Bull et al., 2000), enclosed seas, as the Mediterranean Sea (Kemp et al., 1999;
81 Corselli et al., 2002) and Black Sea (Pilskaln and Pike, 2001), the Southern Ocean (Grigorov et al.,
82 2002; Alley et al., 2018; Tesi et al., 2020).

83 In their study on Pleistocene laminae from the Santa Barbara Basin, Bull et al. (2000) were
84 able to recognise evidence of El Niño events. These were reflected in the frequency of terrigenous
85 laminae representing the continental runoff caused by the intensified rainfall associated to this
86 phenomenon. In the coastal water of Peru, the modern El Niño Southern Oscillation (ENSO) causes
87 a warming of the subsurface water and the consequent deepening of the thermocline (e.g. Caviedes,
88 1984). This condition modifies the regular Peruvian upwelling regime (the periodicity observed
89 today is of ca. 3 to 7 years; Adamson, 2019), by preventing the south-easterly winds to act on the
90 deep cold and nutrient-rich waters segregated under the deeper thermocline. As a consequence,
91 primary production in surface waters declines, causing the loss of large fishery stocks (during 1997-
92 1998 El Niño event, Peruvian fishery export dropped by 66%), inundations along the coast and
93 droughts in the inlands (e.g. Caviedes, 1984).

94 El Niño Southern Oscillation-like variability has been observed in the laminated diatomites
95 of the Upper Cretaceous Marca Shale, California (Davies et al., 2012). Marty (1988) suggests that
96 Eocene laminated diatomites from Fundo Desbarrancado (Southern Peru) testifies an upwelling
97 regime already taking place during the Eocene. Most recent studies based on reconstructing the
98 Pacific surface temperature measuring the Mg/Ca ratio on foraminifera tests have highlighted the
99 presence of the El Niño phenomenon during the Pliocene (Ravelo et al., 2006, 2014 and references
100 therein; White and Ravelo 2020a, b and references therein). These studies suggested us that the
101 investigation of the Miocene diatomaceous laminae of the Pisco Fm may have helped us found the
102 climatic mechanisms that regulated the seasonal stratification of the water column in the area.

103 As a second step, we have wanted to test the possibility of getting indications of the role
104 played by the flux of diatoms to the sea bed in preserving the carcasses and thus leading to the
105 formation of the Lagerstätte. We can get a glimpse of the importance of this Lagerstätte in terms of:
106 1) number of findings by citing the data reported by Bianucci et al. 2016a, b, where the authors list
107 more than 300 specimens preserved as bone elements belonging mostly to cetaceans at the site of
108 Cerro Colorado (Pisco Fossil Lagerstätte Ica Desert, Peru) and 192 fossils of marine vertebrates
109 preserved as bone elements at CLQ; 2) the exceptional preservation of the specimens, both in terms
110 of completeness and details of delicate features such as baleens (e.g., Esperante et al., 2015; Bosio
111 et al., 2021b; Collareta et al., 2021), and; 3) the scientific relevance of this findings by recalling that
112 the Miocene represents a pivotal moment in the evolution of marine vertebrates (Marx and Uhen,
113 2010).

114 Recently, researches have investigated the mechanisms that have favored the fossilisation of
115 all these organisms. Brand et al. (2004) and Esperante et al. (2008, 2015) were the first to
116 hypothesize some of the mechanisms that may have led to the development of the Lagerstätte, citing
117 early mineralisation of the carcasses due to the rapid burial and sedimentation rates in the Pisco Fm
118 two to four orders of magnitude higher than in modern analogues. The mechanism invoked to
119 justify such a high sedimentation rate is a “strong ocean upwelling” (Esperante et al., 2015), which,
120 according to the authors, is indicated by the abundance of the diatom species *Thalassionema*
121 *nitzschiodes*. Yet, neither Esperante et al., (2008, 2015), nor Brand et al. (2004) present in their
122 papers diatom species counts or age models.

123 Only some more recent papers (Gariboldi et al., 2015, 2017; Gioncada et al. 2016, 2018a, b;
124 Bosio et al., 2021a, b) explored in detail the cause of the rapid mineralisation of the carcasses and
125 the sedimentation rates in the Pisco Fm. In particular, Gariboldi et al. (2017) were able to calculate
126 the sedimentation rate of a stratigraphic section measured at CLQ, this being equal to 19 ± 1 cm/ka.
127 This estimate is high, but not exceptional if compared with sedimentation rates of other high
128 productivity basins. However, we must underline that it was calculated using few tie points (either
129 diatom bioevents or $^{40}\text{Ar}/^{39}\text{Ar}$ ages from volcanic ash layers). Considering this limit, we decided to
130 expand our knowledge on the influence of diatom deposition on fossil preservation, by studying in
131 detail the diatomaceous laminae characterising part of the stratigraphic section at CLQ. Such
132 approach provides estimates of the annual sedimentation rates in the basin during the deposition of
133 diatomites, by recognising the annual repetition of species blooms in the sediments: the thickness of
134 annual sequences corresponds to the yearly sedimentation rates.

135 As such, although our information are limited to a small sample, in this paper we debate on
136 the paleoclimatic significance of the CLQ laminae sequences and conclude presenting the
137 implications that the sedimentation rates of the diatomaceous laminae had on the formation of the
138 fossil Lagerstätte.

139

140 2. MATERIALS AND METHODS

141

142 The Pisco Fm crops out along the southwestern coast of Peru, from Pisco to Yauca (ca. 300 km,
143 Fig. 1A), for about 300 km, with a thickness ranging from 200 to 1000 m (Dunbar et al., 1990). It
144 was deposited during the Mio-Pliocene, resulting as the youngest sedimentary unit filling the East
145 Pisco forearc basin (Thornburg and Kulm, 1981; De Muizon and DeVries, 1985; DeVries, 1988,
146 which started to uplift in the Pliocene, mostly due to the subduction of the aseismic Nazca ridge
147 under the South American plate (Hsu, 1992). Nowadays, the East Pisco Basin belongs to the so-
148 called “Pampas Costera” (Coastal Desert), a desert region cluttered with numerous hills with a large
149 base and a planar top (Montoya et al., 1994) and with their stratigraphical top characterised by
150 laminated diatomites (but also by nodular dolomite layers, terrigenous sandstones, tuff beds and
151 phosphorites: Dunbar et al., 1990; Brand et al., 2011; Di Celma et al., 2016; Malinverno et al., 2023).
152 Cerro Los Quesos, CLQ, is one of these hills.

153 After numerous field campaigns undertaken between 2007 and 2015, a total of 192 fossil
154 marine vertebrates were censused at CLQ in an area of approximately 4 km² (Bianucci et al., 2016b).
155 Information, such as the specimens' position, taxonomy, degree of completeness, degree of
156 articulation and potential presence of dolomite nodule enclosing the bones were collected on
157 dedicated sheets (Gariboldi et al., 2015).

158 The stratigraphic position of the fossils was based on the geological investigation and
159 mapping carried out at CLQ by Di Celma et al. (2016). These authors subdivided the sedimentary
160 succession exposed at CLQ in 6 informal lithological members that were labelled from A to F in
161 stratigraphic order. The vertebrate census allowed to point out that 92.7% of the fossils are
162 preserved in the "F member", which is composed mainly of a monotonous succession of finely
163 laminated white diatomites (Di Celma et al., 2016). Considering that, due to the paucity of tie
164 points, specific sedimentation rates were not calculated for each informal member (Gariboldi et al.,
165 2017), in this study we try to identify seasonal laminae cycles in the F member to calculate the
166 yearly accumulation rates of sediments into the basin during its deposition.

167 Using a metal conduit, a 25-cm-thick sample of laminated diatomaceous mudstone was
168 collected in the F member of the CLQ stratigraphic succession, from under a vertebra of a fossil
169 whale (Fig. 2A) called CLQ M58 (Fig. 2; hereafter M58. Specimen position: 14°30'58.3"S;
170 75°43'04.5"W; 167.0 m above the base of the measured section (abs), Bianucci et al., 2016b).
171 The conduit was placed on the outcrop surface and sediments were excavated around the conduit
172 profile. In this way, the conduit slid into the outcrop encapsulating the intact sediment section.
173 Next, the protected sample was dug out of the outcrop. This technique facilitated the preservation of
174 the 25-cm sequence and its stratigraphy. The sample was named CLQ20 (Fig. S1). Besides the fact
175 that M58 is located in the F member, we decided to collect the sample for laminae analysis under it
176 because: 1) M58 represents an almost complete and still articulated specimen, therefore
177 representing a good example of exceptional preservation of the Pisco Lagerstätte; 2) the sediments
178 directly underlying M58 are not only laminated, but also characterised by a typical sediment
179 geochemical perturbation (the yellow-black-red sequence described by Gariboldi et al., 2015 and
180 Gioncada et al., 2018a in the frame of the taphonomic studies of the Pisco Lagerstätte; see details of
181 Fig. 2A) derived by diagenetic processes that bring to the precipitation of a dolomite nodule around
182 the whale carcasses, therefore allowing us to have a complete frame of the different taphonomic
183 processes that a carcass can undergo; 3) M58 is located on the top of the CLQ hill, on a
184 morphological plateau that facilitates the access to the specimen, its observation and the sampling
185 of the underlying sediments; 4) stratigraphically, M58 is placed between two dated volcanic ash
186 layers: the older, the so called "Mono" ash layer, has an age of 6.93 ± 0.09 Ma, while the younger
187 has a lower limit of $\geq 6.71 \pm 0.02$ Ma (Di Celma et al., 2016; See TextS1 in Suppl.Mat.), therefore
188 dating M58 and the CLQ20 sample back to the Messinian (Fig. 3). The age of these rhyolitic ashes
189 was provided by ⁴⁰Ar/³⁹Ar dating of biotite (Di Celma et al., 2016).

190 Small, 4-5 cm subsamples of CLQ20 oriented perpendicular to the lamina fabric were
191 embedded in epoxy resin (Araldite 2020) using a vacuum chamber and a total of 15 (Fig. S1)
192 polished thin sections were prepared for scanning electron microscope backscattered electron
193 imagery (BSEI) analysis (Kemp, 1990; Pike and Kemp, 1996a). Thin sections were carbon-coated
194 and analysed in backscatter mode using a Veeco FEI -Philips- XL30 environmental scanning
195 electron microscope in the School of Earth and Environmental Sciences, Cardiff University and a
196 Hitachi TM 3030 SEM at the Department of Earth Sciences, Pisa University. One thousand two
197 hundred and eighty-four BSEI images were taken to construct 20 BSEI photomosaics at 100x, 800x
198 and 2000x magnification; and more than 400 high magnification images were collected. Only some
199 selected images are presented in this work.

200 Laminations were described using 4 parameters: relative bimodality, laminae content
201 (terrigenous or biogenic particles, diatom species composing each lamina), laminae boundaries
202 (straight or wavy, sharp or blunt) and laminae lateral continuity.

203 The relative bimodality is, as described by Grimm et al. (1996), the relative difference in
204 gray value between adjacent laminae. However, differing from Grimm et al. (1996), we evaluated
205 the bimodality from the BSE images and not from X-radiograph. The difference in gray value on a
206 BSE image depends on the atomic number of the element hit by the electron beam. Terrigenous
207 particles have a higher atomic number than the epoxy resin filling the pores of diatoms and
208 therefore appear lighter. As such, as stated by Grimm et al. (1996), high bimodality (HB) couplets
209 are more evident where pure diatomaceous ooze laminae juxtapose terrigenous laminae.
210 Conversely, low bimodality couplets (LB) are made of discernible laminae but with a very low gray
211 contrast (as in the case of two diatomaceous laminae bearing different species associations). An
212 intermediate situation between HB and LB is defined as moderate bimodality (MB).

213

214 3. RESULTS

215

216 3.1. THE CLQ M58 WHALE AND THE CLQ20 SAMPLE: IN SITU AND MACROSCOPIC OBSERVATIONS

217

218 The M58 whale is an indetermined Balenopteroidea censed by Bianucci et al. (2016b) in the F
219 member of the sedimentary succession exposed at CLQ and described as an articulated skeleton
220 with the skull eroded (Table 1 of Gariboldi et al., 2015 and Fig. 2A, B of this work). M58 lies on a
221 yellow portion of diatomites underlain by a black manganese-rich layer and reddish diatomites (Fig.
222 2A, B, black arrowhead) related to geochemical processes activated by the decomposition of the
223 carcass (see Gariboldi et al., 2015; Gioncada et al., 2018a; see in particular paragraph 3.5 and Fig. 5
224 of Gioncada et al., 2018a for explanations). Therefore, we consider the Mn layer as the boundary
225 between sediments influenced by the presence of the carcass (sediments above the Mn layer) and
226 those not influenced by its presence (sediments below the Mn layer). Below the reddish layer the
227 diatomaceous mudstone shows millimetric white-to-dark grey laminations. The CLQ20 sample
228 represents the sediment under M58 from the yellow diatomites to the gray laminated diatomaceous
229 mudstones, which are interrupted near the bottom of the sample by a 5 mm-thick black tephra (Fig.
230 2A, B, black arrow); unfortunately, the latter could not be dated because of the lack of both biotite
231 and sanidine crystals.

232 Detailed field observation of the skull of M58 highlighted that the lamination was deformed
233 and in some points cut by the Mn layer (Fig. 2B). This deformation strongly resembles the shape of
234 the side of the skull lying on the diatomites and, as suggested by Bosio et al. (2021b), could be the
235 evidence of the sinking of the carcass into the soupy but plastic diatomitic sediments as it reached
236 the seabed.

237

238 3.2. SEDIMENT BIMODALITY, LAMINAE CONTENT, STYLES, SEQUENCES, AND LAMINAE THICKNESSES

239

240 Visual analysis of the low magnification mosaics (100 x) was used to give a general evaluation of
241 the bimodality pattern of the sediment. The sediment appears to be mainly characterized by low to
242 moderate or moderate bimodality (L-MB or MB; Figs. 4A; 5A; 6A; 7A), which is mostly given by
243 the sparse presence of silt particles. Silt particles appear very light in BSE images, within a
244 dominant dark matrix made of the siliceous diatom frustules (Figs. 4C, D, G, J; 5C, D, E, F, H, J, L,
245 M; 7D, E, F; 8G, H). Only rarely the bimodality is high (HB) and this condition is always verified
246 where the terrigenous components dominated by clay particles are grouped to form laminae
247 overlying and overlaid by biogenic ones (Figs. 6A; 7A; 8A).

248 On the basis of the laminae content we can identify:

249

- 250 - terrigenous laminae: laminae where terrigenous particles are > 90% of the laminae. In
251 CLQ20 these laminae are mostly made by clay particles (Figs. 6B, E; 7B, C, F; 8D, E, F),
252 but also some silt particles (Figs. 8A, D) or biogenic particles, such as rare *Thalassionema*
253 specimens (Fig. 6C), or other species (Fig. 8D).

254
255
256
257
258
259
260
261
262
263
264
265
266
267
268
269
270
271
272
273
274
275
276
277
278
279
280
281
282
283
284
285
286
287
288
289
290
291
292
293
294
295
296
297
298
299
300
301
302
303
304

- *Coscinodiscus* laminae: in this paper we use the definition “*Coscinodiscus* lamina” to indicate a diatomite (a hard pelagic sediment made by >30% of skeletal remains of diatoms and <30% silt and clay, as defined by Palmer et al., 1986) where *Coscinodiscus* (possibly *Coscinodiscus asteromphalus*; Tab. 1) is the dominant genus (>90%; figs. 4B, E; 5B, F, G, I, K, M; 8A, C, G). Other rare components of these laminae are *Actinocyclus octonarius* (Tab. 1) specimens (Fig. 4F), *Thalassionema* specimens (Fig. 8B; Tab. 1) and rare terrigenous particles (Fig. 4E).
- Mixed laminae (Figs. 4A, B, G, H, I, J; 5A, B, C, D, E, H, J, L; 6A, B; 7A, D, E, F; 8A, H): these are laminae composed of clay and silt particles in different percentages (Figs. 4B, C, D, G; 5B, C, D, E, H, L, J; 7D, E, F; 8A, H), specimens of *Coscinodiscus* (Figs. 4B, J; sometimes the presence of *Coscinodiscus* in mixed laminae is due to an interdigitation of *Coscinodiscus* laminae with mixed laminae as in Fig. 5L) *Actinoptychus* (Figs. 4H; 5D, red circle, probably *Actinoptychus senarius*; Tab. 1), *Stephanopyxis* (most probably *Stephanopyxis turris*, Figs. 4G, J; 5E, red circle; Tab. 1) and *Chaetoceros Hyalochaete* spp. resting spores (CRS; Figs. 4I; 8H; Tab. 1). The percentages of these different components vary in each mixed lamina.
- *Actinoptychus* cf. *senarius* laminae: rare diatomites where *Actinoptychus* cf. *senarius* represents >90% of the diatom species (Figs. 6A, D, E; Tab. 1).

Straight lamina boundaries in sample CLQ20 are rarely found and difficult to be traced, as the transitions from one lamina to the next are often indistinct. More frequently, boundaries are wavy (Figs. 4B; 5B; 6D) and, as said, indistinct, especially when representing the limit between a diatomaceous lamina and a mixed lamina (Figs. 4A, B). Only in slide t14 quite distinct boundaries between a *Coscinodiscus* lamina and the over- and underlying mixed laminae are recognisable at low magnification (Fig. 5A, dotted lines). Noteworthy, the only sharp boundaries are those delimiting terrigenous clayey laminae from others (Figs. 6A, B; 7A; 8A). Boundaries between these laminae and the others are normally less wavy (then those between biogenic laminae) or straight (Figs. 6A -white arrows-; 7A; 8A); also clots of clay can be observed throughout some slides, resembling a terrigenous lamina, but having a boudinage-like aspect (Figs. 6A -arrowheads-; 7A -arrowheads and arrows on the right side of the figure-). We do not consider them laminae as they are very thin (also << 100 µm). These clots have very straight and distinct boundaries, just as terrigenous laminae (Figs. 7B, F).

Both composition and boundaries of laminae help in verifying if they are laterally continuous; in CLQ20, although boundaries are normally indistinct, they are typically continuous (Figs. 4A; 5A; 6A; 7A; 8A) and discontinuous laminae are present.

A deeper investigation at 800 x and 2000 x magnification helped the identification of different sequences of laminae, in particular:

- the mixed lamina-*Coscinodiscus* lamina duplet (Figs. 4B; 5B; S2)
- the terrigenous lamina-*Coscinodiscus* lamina duplet (Fig. 8A);
- the mixed lamina-*Actinoptychus* cf. *senarius* lamina duplet (Figs. 6A, D, E).

The last case was observed only once and, therefore, it is considered rare. Also the terrigenous lamina-*Coscinodiscus* lamina duplet is evident only in one case (Fig. 8A). In Fig. 7A some clots of clay topping the mixed laminae can be observed (arrows on the right of the photo); these have a frequency of 3-3.5 mm, made exception for the first one, which is ca. 1 mm apart from the underlying terrigenous lamina. Similar clots overlying a mixed lamina are observed in slide t5 (Fig. 6A -arrowheads-, E).

Comparing at higher magnification (Fig. S2) the t9 slide (Fig. 7A) for its whole length it appears clearly that the sediment is mainly composed of the mixed lamina-*Coscinodiscus* lamina

305 duplet, the mixed laminae being topped by clay clots (Fig. 7A –arrows-; S2 –arrows-). As the t9
306 slide is defined by a MB (Fig. 7A) we consequently translated the MB and L-MB feature (Figs. 4A;
307 5A; 7A) into sediment composition: in other words, we started considering the MB and L-MB
308 equivalent to the presence of mixed lamina-*Coscinodiscus* lamina duplet. This deduction is
309 confirmed by the investigations at higher magnifications of slides t13, t14, t9 images (800 x and
310 2000 x: Figs. 4B; 5B, 8A), where this duplet prevails. As the L-MB and MB are the mostly
311 observed throughout the CLQ20 sample, we deduce that the mixed lamina-*Coscinodiscus* lamina
312 duplet is the one most frequent in CLQ20.

313 The mixed lamina-*Coscinodiscus* lamina duplet shows very different thicknesses, the three
314 highlighted in Fig. 5B varying from ca. 625 μm to ca. 1750 μm , with a huge difference in the
315 thickness of the two mixed laminae (ca. 375 μm in the second duplet vs. ca. 1500 μm in the third
316 duplet). Differences in the thickness of *Coscinodiscus* laminae are nonetheless noteworthy: on one
317 hand, the *Coscinodiscus* lamina of the second and third duplets are similar (varying from ca. 250
318 μm to 500 μm); on the other hand the *Coscinodiscus* lamina of the first (highlighted with an
319 asterisk) and second duplets are ca. 1000 μm thick (Fig. 5B). The lower boundary of the mixed
320 lamina of the first duplet is not clear, therefore we do not report the thickness of the whole duplet.
321 Significantly, also in the duplet terrigenous lamina-*Coscinodiscus* lamina observed in Fig. 8A, the
322 latter is ca. 250 μm as in the two cases in Fig. 5B; its terrigenous companion is ca. 650 μm thick
323 (Fig. 8A), the thickness of the whole duplet being ca. 900 μm .

324 4. DISCUSSION

325 4.1. PALEOCLIMATIC IMPLICATIONS OF THE PISCO FM. DIATOM LAMINAE

326
327
328
329 There are at least three features confirming that laminae in the CLQ20 sample are the product of a
330 primary deposition process: i) the recurrent patterns of laminae in the CLQ20 sediments, in
331 particular the mixed lamina-*Coscinodiscus* lamina; ii) the very well-defined boundaries of the
332 terrigenous laminae; and iii) the lateral continuity of laminae.
333 The characteristic of the primary production inputs and of the terrigenous ones, can therefore be
334 used as proxy for a paleoclimatic reconstruction of the area.

335 The studies of laminated sediments from the Peru forearc basins (Kemp, 1990; Brodie and
336 Kemp, 1994) described upper Quaternary laminated sediments from the Peru shelf and upper slope.
337 These were collected during ODP Exp 112 (Sites 680, 681 and 686) and during the R.R.S. Darwin
338 Leg 38 (Sites 38.10 and 38.9). These studies highlighted the presence of three different groups of
339 laminae; isolated, irregularly spaced and continuous sub-millimetre laminae. In all those three cases
340 diatomaceous laminae are often mainly monospecific and composed of upwelling genera, such as
341 *Skeletonema* and *Chaetoceros*. Conversely, *Coscinodiscus* oozes are rare. On the other hand,
342 terrigenous laminae are either silt-rich (main thickness 600 μm , with a standard deviation of 350
343 μm) or clay-rich laminae (main thickness 550 μm , with a standard deviation of 500 μm), with the
344 silt component not invariably present in the sequence (Brodie and Kemp, 1994). These laminae
345 form a sub-millimetre couplet that is irregularly inter-laminated with diatom ooze. The oozes are
346 controlled by the intensity of upwelling and/or the nutrient content of upwelled waters, while
347 terrigenous laminae are the expression of regular rainfalls caused by the permanent presence of
348 warm water off Peru during Isotope Stage 5 (Brodie and Kemp, 1994). The absence of diatom oozes
349 between the silt/clay couplets is interpreted by the authors either as the result of absence of an algal
350 bloom or the complete dissolution of the crop in the water column; both these hypotheses would
351 suggest a reduction of nutrient availability, a feature which is consistent with El-Niño events
352 (Brodie and Kemp, 1994).

353 *Coscinodiscus* spp. were associated with the “Fall dump” events, described for the first time
354 in the Gulf of California, during the Holocene, by Kemp et al. (2000). The authors identify
355 *Coscinodiscus* spp. specimens as “clusters of individuals rather than as contiguous sub-laminae”

356 deposited above the diatomaceous laminae (made either of *Rhizosolenia* spp. or *Stephanopyxis*
357 *palmeriana*) overlying the summer terrigenous lamina. Therefore, the authors include this genus
358 among those that are able to thrive at the thermo/nutricline at low light conditions preferring a
359 stratified water column, the so-called “shade” flora (Sournia, 1982; Kemp et al., 2000). Blooms of
360 the “shade flora” may last throughout the periods of water stratification; the diatoms growing during
361 this period start settling with the onset of fall/winter mixing (the “fall dump”) (Kemp et al., 2000).
362 These characteristics make them differ from the small subgenus *Chaetoceros Hyalochaete*, which
363 thrives during upwelling conditions (spring) (Kemp et al. 2000). Somehow similarly, Romero and
364 Hebbeln (2003), studying diatom assemblages of surface sediments below the Peru-Chile Current,
365 list *Chaetoceros* species in the coastal upwelling group (together with *Thalassionema nitzschioides*
366 var. *nitzschioides*), while they classify *Coscinodiscus argus* and *C. radiatus* in the coastal
367 planktonic group (characterised by the presence of non-upwelling associated species). Yet, the
368 authors find *C. argus* and *C. radiatus* together with *Chaetoceros* spp. between 34° and 38° S,
369 highlighting that at those latitudes the primary production is due to both upwelling and proliferation
370 of the fall dump flora during periods of water column stratification.

371 With these pieces of information, some interpretations can be given to the *Coscinodiscus*
372 laminae, while no present analogue has been observed for the *Actinoptychus* cf. *senarius* lamina
373 (Figs. 6A, D, E).

374 Indeed, the huge contribution of *Coscinodiscus* spp. to the diatom fraction in laminae of
375 sample CLQ20 and the scarce presence of *Chaetoceros Hyalochaete* spp., which was observed only
376 in small sparse clusters (Figs. 4I, 8H), testify that primary production during the deposition of the F
377 member was regulated by the stratification of the water column rather than by coastal upwelling;
378 however, the presence of both phenomena in the same region, during different time of the year, is
379 also plausible.

380 On one hand, the absence of *Rhizosolenia* spp. and *Stephanopyxis palmeriana* in the fall
381 dump lamina suggests that the dominance of *Coscinodiscus* is not only related to stratification of
382 the water column but also to some other ecological limiting factor. As *Stephanopyxis palmeriana* is
383 known as a warm water (Drebes, 1966) tropical species (Molina et al., 1997), warmer than
384 *Stephanopyxis turris* (Cupp, 1943), a species sporadically present in the CLQ20 sediments (Figs.
385 4B, G; 5E, L), it appears that water temperature may play a role in the absence of *S. palmeriana*.
386 More generally, it can easily be assumed that the waters present in the Eastern Equatorial Pacific
387 (EEP) Ocean during the late Miocene had different properties and origin in respect of those present
388 in the Gulf of California during the Holocene; as such, it is not surprising that the dominant genera
389 thriving at the thermocline in these two scenarios are different. Also Shankle et al., (2020) tested the
390 possibility that water properties reaching the equatorial Pacific in the Late Miocene/Early Pliocene
391 were different from today’s (older, more acid and more nutrient-rich).

392 On the other hand, the absence of strong upwelling-related-*Chaetoceros* blooms, such as
393 recorded in the laminae of the CLQ20 sample, may reflect a deepening of the thermocline in the
394 EEP during the Messinian. Currently, this condition is registered during El Niño events: during the
395 1982-1983 El Niño, the winds were constantly upwelling-favourable but the thermocline was
396 deeper than normal. Thus, as the source depth of upwelled water was the same of normal conditions
397 (i.e. 50-100 m), upwelled waters were warm and poor of nutrients, as they came shallower than the
398 thermocline (Huyer et al., 1987). Such a functioning of the El Niño was later confirmed by other
399 authors (Strub et al., 1998; Hill et al., 1998).

400 With these observations in mind, when looking at the CLQ20 mosaics one may be tempted
401 to say that the mixed lamina-*Coscinodiscus* lamina duplets, together with the terrigenous lamina –
402 *Coscinodiscus* lamina duplets are not only the expression of a El-Niño like condition, but, indeed of
403 the El Niño condition itself (or, at least, of a proto El-Niño condition). Not only the paucity of CRS,
404 together with the abundance of *Coscinodiscus* ssp., highlights a stratified water column with warm
405 and nutrient-poor upwelled water: also the presence of silt particles in mixed laminae point to a
406 rainy condition, which appears to increase its intensity periodically (as described by Bull et al.,

407 2000, for late Quaternary in the Santa Barbara Basin and as it is known to happen today during El
408 Niño phenomena; see for examples Caviedes, 1984; Hebbeln et al, 2000; Romero et al., 2002; Shipe
409 et al 2002) leading to the formation of clots of clay (Figs. 7A –arrows-; Fig. S2 –arrows-). Briceño-
410 Zuluaga et al. (2016) gave to the enhanced particle flux observed in the Pisco Basin during the
411 Little Ice Age a similar interpretation.

412 Although aware that such affirmation is far too reckless (more data would be needed for
413 such a statement), we still think that this observation may encourage to start to look better into
414 diatomaceous records that may help us comprehend when and how the ENSO phenomenon started.

415 At present the El Niño phenomenon has been identified back to the Cretaceous (Davies et
416 al., 2012) and to the so called “Middle Pliocene Warm Period”, ca. 4.5 – 3.0 Ma (Wara et al., 2005;
417 Fedorov et al., 2006; Ravelo et al., 2006; Ragaini et al., 2008; White and Ravelo, 2020a, b. See
418 TextS2 in Suppl.Mat.). Some authors stated that, during the Middle Pliocene Warm Period the El
419 Niño conditions was permanent, rather than showing a periodicity similar to that of recent days: this
420 is the so called “El Padre” state (Ravelo et al., 2014), which is not a individual event, like El Niño,
421 but a “mean state”. The deepening of the thermocline and, therefore, the phenomena of El Niño, is
422 triggered by the warming of the EEP and by the consequent drop of the temperature gradient
423 between the Western Pacific Warm Pool and the EEP (Wara et al., 2005; Zhang et al., 2014a),
424 consisting in a mean zonal gradient in the case of El Padre.

425 The hypothesis on whether the El Padre state either existed or is just a result of a bias in the
426 proxies (TEX₈₆, U^K₃₇, Mg/Ca) used for the reconstruction of the SST gradient is still ongoing
427 (Zhang et al., 2014a, b; Ravelo et al., 2014; White and Ravelo 2020b, and reference therein), also
428 extending into the Middle Miocene (Fox et al., 2021).

429 Although the discussion on the existence of an El Padre State lies outside the objectives of
430 this paper, we would like to point out that: 1) there is no doubt that the CLQ20 *Coscinodiscus*
431 laminae point to a deepening of the thermocline in the Messinian and it is stunning to observe that
432 the deposition of CLQ20 happened during a period when SST in the EEP were increasing (Fig. 3)
433 and 2) a primary production segregated at the thermocline depth may help explain the so-called
434 “Pliocene paradox” (Shankle et al., 2000), which highlights enhanced primary production in the
435 EEP despite a reduced latitudinal gradient (which, as said, would imply a deepening of the
436 thermocline in the EEP) in the Late Miocene/Early Pliocene; and 3) the BSE images of CLQ20
437 highlights that shade flora can represent a huge percentage of the total diatom assemblage;
438 therefore, given the importance of the carbon export attributable to the thriving of the shade flora at
439 depth, the use of biogenic silica as a proxy for intensification of upwelling, as done in some
440 researches (for example, Holbourn et al., 2014; Fox et al., 2021. Also Esperante et al., 2015 suggest
441 that the abundant occurrence of *Thalassionema nitzschioides* in the sediment of the Pisco Fm.
442 suggests strong upwelling conditions) should not be used without a quantitative check of the
443 different diatom species present in the sediment.

444 To conclude, it is vital to point out what climate modeling suggests us: to an increase in
445 atmospheric CO₂, models point out a reduction of the temperature gradient between the Western
446 Pacific Warm Pool and the EEP, caused by an enhanced warming of the EEP compared to the West
447 Pacific (Meehl and Washington, 1996); as such, the current increase of CO₂ in the atmosphere, may
448 lead to a future characterised by more frequent El-Niño events (Meehl and Washington, 1996).

449 4.2. THE ROLE OF DIATOM LAMINATIONS IN PRESERVING MARINE FOSSIL VERTEBRATES

451
452 The investigation of diatomaceous laminae of the CLQ20 sample, the recognition of some laminae
453 sequences that may be assumed as annual cycles (literally the mixed lamina-*Coscinodiscus* lamina
454 and the terrigenous lamina-*Coscinodiscus* lamina duplets) and the possibility of measuring their
455 thickness, open a further discussion on their role in favoring the preservation of marine fossils in the
456 F member of the Pisco Fm at CLQ. The sedimentation rates registered along the F member
457 (approximately 500 µm to 2 mm/a for the mixed lamina-*Coscinodiscus* lamina duplet, Fig. 5B; 900

458 μm for the terrigenous lamina –*Coscinodiscus* lamina duplet, Fig. 8A), although supported by few
459 data, are conspicuously different from those calculated for the whole section at CLQ, at least
460 doubling and sometimes even increasing of one order of magnitude those previously reported by
461 Gariboldi et al, 2017 (0.2 mm/a of Gariboldi et al. 2017 for the CLQ section vs. 0.5 to 2 mm/a (50
462 to 200 cm/ka) for the F member, this study). Differing from Gariboldi et al., (2017), who took in
463 account a compaction of the sediments equal to 60% (by giving a wrong interpretation to Isaacs et
464 al., 1983), in this paper we consider a definitely lower porosity loss for diatomaceous sediments due
465 to compaction: Hamilton (1976) calculated a porosity loss during early burial of diatomaceous
466 sediments equal to 15% (from 86% to 71% at 500 m below sea floor). Adding this 15% to the
467 thickness of laminae observed in CLQ20 would implicate an insignificant increase to the yearly
468 sedimentation rates. This implies that only in some cases these sedimentation rates are higher than
469 those of Quaternary basins where primary production is high (e.g. Pleistocene of DSDP Site 478,
470 Gulf of California, DSDP Leg 64, > 125 cm/ka, Schrader 1982; Quaternary of ODP Site 686, West
471 Pisco Basin, ODP Leg 112, 16 cm/ka Suess and Von Huene 1988; Pleistocene of ODP Site 1078
472 outside the Bight of Angola, ODP Leg 175, 60 cm/ka, Wefer et al. 1998; Pleistocene of ODP Site
473 881, 5.6 cm/ka and Mio–Pliocene of ODP Site 883, 9.1 cm/ka, Subarctic Pacific Ocean, ODP Leg
474 145, Rea et al. 1993); to this list we add the sedimentation rates recorded in the last 2.6 ka old
475 sediments of the Edisto Inlet, Ross Sea, Antarctica: Tesi et al. (2020) calculated a sedimentation
476 rate equal to 2 to 7 mm/a (200 to 700 cm/ka) for the laminated diatomaceous sediment of core
477 HLF17-01. As, due to their lithology and fabric, diatomaceous sediments of the Edisto Inlet may be
478 considered a modern analogue of sediments from the F member, it is worth reporting that in core
479 ANTA02-CH41, Edisto Inlet, the soupy consistence of the diatomaceous laminated mud revealed a
480 water content that was close to 80% (Finocchiaro et al., 2005). Imaging such physical characteristic
481 for a just-deposed diatom ooze at the bottom of the East Pisco Basin would itself explain how deep
482 marine vertebrate carcasses may have sunk into the sediments, supporting the “impact burial”
483 (partial or complete burial of an object in the sediments upon its high velocity sinking through the
484 water column into soupy substrates) hypothesis proposed by Bosio et al. (2021b) to explain the
485 rapid burial of marine vertebrates in the Pisco Fm. Indeed, any of the sedimentation rates calculated
486 in this paper and in Gariboldi et al., 2017 are not high enough to cover large carcasses permitting
487 high articulation and high completeness of the fossil specimens, as observed in the Pisco Fm
488 (Gariboldi et al., 2015). As such, we agree with Brand et al. (2004), who state that rapid burial is
489 needed to explain such a preservation in the Pisco Fm. However, we disagree when they state that
490 “such burial requires diatom accumulation rates at least three to four orders of magnitude faster than
491 is usual in the ocean today—centimeters per week or month, rather than centimeters per thousand
492 years”. Also, Gariboldi et al. (2015) highlighted the role of dolomite precipitation inside and outside
493 (dolomite nodule) the whale carcasses in the process of preservation of the fossils (for example, by
494 avoiding bone dissolution, preventing diagenetic compression of the specimens and erosion of
495 bones, favoring the articulation and completeness of skeletons). The process of dolomite
496 precipitation, which also includes recurrent basin-wide decimetric-thick dolomite layers
497 (Malinverno et al., 2023), was explained as biomediated by sulphate-reducing bacteria, which are
498 able to degrade organic matter in low-oxygen environment, as demonstrated also in laboratory
499 experiments (see references therein Gariboldi et al. 2015). Thus, the sinking of the carcasses into
500 the soupy diatom ooze would have favored the formation of the Pisco Lagerstätte also by
501 subtracting the carcasses from a possible oxygenated sea floor, thus favoring dolomite precipitation.

502 503 4.3 CLQ20: THAT’S ONE SMALL SAMPLE FOR A FORMATION

504
505 We need to recall to the readers that the CLQ20 sample is a very short piece of the diatomite
506 portion of the P2 allomember of the Pisco Fm and that it may be representative neither of the whole
507 F member, nor of the diatomitic portions of the other older and younger allomembers of the Pisco
508 Fm (Lamy et al., 2001, affirm that changes in continental rainfall in southern Chile are regulated by

509 millennial to multi-centennial shifts in the position of the southern westerlies, periods that lag far
510 behind the duration of the CLQ F member deposition). However, in their studies of the
511 biostratigraphy of the Pisco Fm, Gariboldi et al., (2017) have published a table of relative
512 abundances for all the diatom species encountered in the Cerro Los Quesos; from this work (table 3
513 of Gariboldi et al., 2017; see TextS3 in Suppl.Mat.) we can infer that *Coscinodiscus asteromphalus*
514 is present in great abundance in almost all the samples collected in the CLQ F member; yet, also
515 CRS are always present. This apparent equality between these two genera abundances can be
516 explained considering the counting method (Schrader and Gersonde, 1978; Armand, 1997; Crosta
517 and Koç, 2007); following this protocol only *Coscinodiscus* spp. valve which are preserved for $\frac{3}{4}$ or
518 more can be counted in the assemblage. However, the higher valve-face diameter/pervalvar-axis
519 ratio makes large diatoms easier to break during slide preparation, resulting at last in an
520 underestimation of large diatoms in the assemblages. Conversely CRS are often found intact, with
521 the 2 valves still connected.

522 As such, it appears clear that analyses on diatom assemblages by means of the light
523 microscope, combined with those on diatom laminations, where possible, may be the most direct
524 proxy, yet imprecise (as they give no absolute values on the reduced zonal SST gradient), to study
525 the initiation and the temporal patterns of ENSO in the deep time and to verify the hypothesis of the
526 El Padre state. The observation of laminae in their original depositional settings gives a glimpse, not
527 only on the depositional mechanism, but also on the real relative abundance of different species;
528 light microscope analysis is essential to investigate long stratigraphic succession efficiently.

529
530

531 5. CONCLUSIONS

532

533 Backscattered electron imagery analysis of Cerro Los Quesos laminated diatomaceous mudstone
534 provided insight into the seasonality that was affecting water column stability.

535 The most frequent laminae duplet observed in the Messinian CLQ20 sample is the mixed
536 lamina – *Coscinodiscus* lamina duplet. The large contribution in the CLQ20 sediments of this
537 duplet, and of the genus *Coscinodiscus* in general (also in the less frequent terrigenous lamina –
538 *Coscinodiscus* lamina duplet), reflects a rather deep position of the thermocline. This water column
539 setup led to a weak proliferation of upwelling related diatom species (i.e., *Chaetoceros Hyalochaete*
540 and *Thalassionema*), as the upwelled waters were warm and nutrient-poor. Such oceanographic
541 situation resembles that hypothesized for the so-called “El Padre” state in the middle Pliocene
542 Warm Period; this is described as a constant El Niño phenomenon (a “mean state”) triggered by the
543 warming of the EEP and the consequent drop of the temperature gradient between the West Pacific
544 Warm Pool and the EEP itself. As such, we highlight that: 1) studies focused on verifying the
545 existence of the El Padre setup in the low latitude Pacific during the Late Miocene are needed; and
546 2) climate modelling suggests that to a future increase in atmospheric CO₂ will correspond an
547 enhanced warming of the EEP compared to the West Pacific, which may lead to more frequent El-
548 Niño events.

549 Analyses on CLQ20 laminae thickness have confirmed that sedimentation rates in the Pisco
550 Basin during the Late Miocene were comparable to those of Quaternary basins elsewhere. This
551 evidence rules out the hypothesis that depositions of diatomites in the East Pisco Basin were orders
552 magnitude faster than in today’s oceans. Moreover, direct observation on modern diatom oozes and
553 the observation made on their water content, make us affirm that the hypothesis of an “impact
554 burial” for the marine vertebrate carcasses is robust.

555 On a broader view, our study suggests that:

556

- 557 - during diatom counts for palaeological analysis, special care should be paid in not
558 underestimating large-sized diatoms over small-sized ones; light microscope analysis coupled
559 with BSEI analysis on diatom laminations (where possible) helps overcome this possible bias;

- 560 - analyses on diatom assemblages and diatom laminations, where possible, may be the most direct
561 proxy, yet imprecise (as it gives no absolute values on the reduced zonal SST gradient), to study
562 ENSO in the deep time;
563 - the use of biogenic silica as a proxy for intensification of upwelling, as done in some researches,
564 should be used with caution, given the importance of the carbon export attributable to the
565 thriving of the shade flora at depth.

566

567 OPEN RESEARCH

568

569 BSE images are from Gariboldi et al. 2023, available at
570 <https://doi.org/10.6084/m9.figshare.22309204.v1>. Data used to compile Fig. 3 are available from
571 Rousselle et al., 2013 and Herbert et al., 2016.

572

573 ACKNOWLEDGMENTS

574

575 We would like to thank Anthony Oldroy, Peter Fisher, Lindsey Axe and Duncan Muir (School of
576 Earth and Ocean Sciences, Cardiff University) for the help during sample preparation and SEM
577 analyses. We would also like to thank Prof. John Barron and Prof. Carina Lange for their constant
578 support and for the many productive discussions. This study was supported by grants from the
579 Italian Ministero dell'Istruzione dell'Università e della Ricerca (PRIN Project 2012YJSBMK to G.
580 Bianucci), by a National Geographic Society Committee for Research Exploration grants (9410-13
581 to G. Bianucci), and the University of Camerino (FAR 2019, STI000102 to C. Di Celma). K.G.
582 would like to thank Caterina Morigi, Alessandra Negri and Giacomo Galli for their help in
583 improving the manuscript. We would like to thank the Editor, Ursula Röhl Associated Editor, Alex
584 Farnsworth,

585 and the anonymous Reviewers for the precious observations that have helped us improving the
586 manuscript and Editor's Assistant, Meghan Ramil, for the technical assistance during the peer-
587 review process. This work is dedicated to those we lost during the COVID-19 pandemic.

588

589 REFERENCES

590

- 591 - Abrantes F., Lopes C., Mix, A., & Pisias N. (2007). Diatoms in Southeast Pacific surface
592 sediments reflect environmental properties. *Quaternary Science Reviews*, 26(1-2), 155-169.
- 593 - Adamson G. (2019). El Niño and society. In *Oxford Research Encyclopedia of Climate Science*.
594 Oxford University Press.
- 595 - Alley K., Patacca K., Pike J., Dunbar R., Leventer, A., (2018). Iceberg Alley, East Antarctic
596 Margin: Continuously laminated diatomaceous sediments from the late Holocene. *Marine*
597 *Micropaleontology*, 140, 56-68.
- 598 - Armand L., (1997). The use of diatom transfer functions in estimating sea-surface temperature and
599 sea-ice in cores from the southeast Indian Ocean. Ph.D thesis, Australian National University,
600 Canberra, Australia.
- 601 - Bianucci G., Di Celma C., Landini W., Post K., Tinelli C., de Muizon C., Gariboldi K.,
602 Malinverno. E., Cantalamessa G., Gioncada. A., Collareta A., Salas-Gismondi R., Varas-Malca
603 R., Urbina M. & Lambert O., (2016a). Distribution of fossil marine vertebrates in Cerro
604 Colorado, the type locality of the giant raptorial sperm whale *Livyatanmelvillei* (Miocene, Pisco
605 Formation, Peru). *Journal of Maps*, 12(3), 543-557.
- 606 - Bianucci G., Di Celma C., Collareta A., Landini W., Post K., Tinelli C., de Muizon C., Bosio G.,
607 Gariboldi K., Gioncada A., Malinverno E., Cantalamessa G., Altamirano-Sierra A., Salas-
608 Gismondi R., Urbina M. & Lambert O., (2016b). Fossil marine vertebrates of Cerro Los Quesos:
609 distribution of cetaceans, seals, crocodiles, seabirds, sharks and bony fish in a late Miocene
610 locality of the Pisco Basin, Peru. *Journal of Maps*, 12(5): 1037-1046

- 611 -Bosio G., Gioncada A., Gariboldi K., Bonaccorsi E., Collareta A., Pasero M., Di Celma C.,
612 Malinverno E., Urbina M., Bianucci G., (2021a). Mineralogical and geochemical
613 characterization of fossil bones from a Miocene marine Konservat-Lagerstätte. *Journal of South*
614 *American Earth Sciences*, 105, 102924.
- 615 - Bosio G., Collareta A., Di Celma C., Lambert O., Marx F. G., de Muizon C., Gioncada A.,
616 Gariboldi K., Malinverno E., Varas-Malca R., Urbina M., Bianucci G., (2021b). Taphonomy of
617 marine vertebrates of the Pisco Formation (Miocene, Peru): Insights into the origin of an
618 outstanding Fossil-Lagerstätte. *Plosone*, 16(7), e0254395.
- 619 - Brand L.R., Esperante R., Chadwick A.V., Poma Porras O., Alomía M., (2004). Fossil whale
620 preservation implies high diatom accumulation rate in the Miocene-Pliocene Pisco Formation of
621 Peru. *Geology*, 32(2): 165-168.
- 622 - Briceño-Zuluaga F.J., Sifeddine A., Caquineau S., Cardich J., Salvattecí R., Gutierrez D., Ortilieb
623 L., Velazco F., Boucher H., & Machado, C. (2016). Terrigenous material supply to the Peruvian
624 central continental shelf (Pisco, 14° S) during the last 1000 years: paleoclimatic
625 implications. *Climate of the Past*, 12(3), 787-798.
- 626 - Brodie I., Kemp A.E.S., (1994). Variation in biogenic and detrital fluxes and formation of laminae
627 in late Quaternary sediments from the Peruvian coastal upwelling zone. *Marine Geology*, 116:
628 385-398.
- 629 -Bull D., Kemp A.E.S., Weedon G.P.A, (2000). 160-k.y.-old-record of El Niño southern Oscillation
630 in marine production and coastal run-off from Santa Barbara Basin, California, USA. *Geology*,
631 28, 1007-1010.
- 632 - Caviedes C. N., (1984). El Niño 1982-83. *Geographical Review*, 267-290.
- 633 - Collareta A., Landini W., Lambert O., Post K., Tinelli C., Di Celma C., Panetta D., Tripodi M.,
634 Salvadori P.A., Caramella D., Marchi D., Urbina M., Bianucci G., (2015). Piscivory in a
635 Miocene Cetotheriidae of Peru: first record of fossilised stomach content for an extinct baleen-
636 bearing whale. *Science of Nature*, 102, 70.
- 637 - Collareta A., Lambert O., Marx F. G., de Muizon C., Varas-Malca R., Landini W., Bosio G.,
638 Malinverno E., Gariboldi K., Gioncada A., Urbina M., Bianucci G., (2021). Vertebrate
639 Palaeoecology of the Pisco Formation (Miocene, Peru): Glimpses into the Ancient Humboldt
640 Current Ecosystem. *Journal of Marine Science and Engineering*, 9(11), 1188.
- 641 - Corselli C., Principato M.S., Maffioli P., Crudeli D., (2002). Changes in planktonic assemblages
642 during sapropel S5 deposition: Evidence from Urania Basin area, eastern Mediterranean.
643 *Paleoceanography*, 17(3): 1-30.
- 644 - Crosta X., Koç N., (2007) – Chapter Eight Diatoms: From Micropaleontology to Isotope
645 Geochemistry. *Developments in Marine Geology*, Volume 1, pp. 327-369.
- 646 - Cupp E.E., (1943). Marine plankton diatoms of the west coast of North America. Otto Koeltz
647 Science Publishers.
- 648 - Drebes G., (1966). On the life history of the marine plankton diatom *Stephanopyxis*
649 *palmeriana*. *Helgoländer wissenschaftliche Meeresuntersuchungen*, 13(1), 101-114.
- 650 - Davies A., Kemp A.E., (2016). Late Cretaceous seasonal palaeoclimatology and diatom
651 palaeoecology from laminated sediments. *Cretaceous Research*, 65, 82-111.
- 652 - Davies A., Kemp A.E., Pike J., (2009). Late Cretaceous seasonal ocean variability from the
653 Arctic. *Nature*, 460(7252), 254-258.
- 654 - Davies A., Kemp A.E., Weedon G.P., Barron, J.A., (2012). El Niño–southern oscillation
655 variability from the late cretaceous Marca shale of California. *Geology*, 40(1), 15-18.
- 656 - De Muizon C., DeVries T.J., 1985. Geology and paleontology of late Cenozoic marine deposits in
657 the Sacaco area (Peru). *Geologische Rundschau*, 74, 547–563.
- 658 - DeVries T.J., 1988. Paleoenvironments of the Pisco Basin. Cenozoic geology of the Pisco Basin.
659 In: Dunbar R.B., Baker P.A. (Eds.), *Cenozoic Geology of the Pisco Basin*. Guidebook, IGCP 156
660 Field Workshop: Genesis of Cenozoic Phosphorites and Associated Organic-rich sediments:
661 Peruvian Continental Margin, pp. 41–50.

- 662 - Di Celma C., Malinverno E., Cantalamessa G., Gioncada A., Bosio G., Villa I.M., Gariboldi K.,
663 Rustichelli A., Pierantoni P.P., Landini W., Tinelli C., Collareta A., Bianucci G., (2016).
664 Stratigraphic framework of the late Miocene Pisco Formation at Cerro Los Quesos (Ica Desert,
665 Peru). *Journal of Maps*, 12(5): 1020-1028.
- 666 - Dudley W.C., Blackwedler P., Brand L., Duplessy J.-C., (1986). Stable isotopic composition of
667 coccoliths. *Marine Micropaleontology*, 10(1-3):1-8
- 668 - Dunbar R.B., Berger W.H., (1981). Fecal pellet flux to modern bottom sediment of Santa Barbara
669 Basin (California) based on sediment trapping. *Geological Society of America Bulletin* 92(4):
670 212-218.
- 671 - Dunbar R.B., Marty R.C., & Baker P.A., (1990). Cenozoic marine sedimentation in the Sechura
672 and Pisco basins, Peru. *Palaeogeography, Palaeoclimatology, Palaeoecology*, 77(3-4), 235-261.
- 673 - Esperante R., Brand L., Nick K., Poma O., Urbina M., 2008. Exceptional occurrence of fossil
674 baleen in shallow marine sediments of the Neogene Pisco Formation, Southern Peru.
675 *Palaeogeography. Palaeoclimatology. Palaeoecology*, 257:344-360.
- 676 - Esperante R., Brand L.R., Chadwick A.V., Poma O., (2015). Taphonomy and paleoenvironmental
677 conditions of deposition of fossil whales in the diatomaceous sediments of the Miocene/Pliocene
678 Pisco Formation, southern Peru - A new fossil-lagerstätte. *Palaeogeography, Palaeoclimatology,*
679 *Palaeoecology*, 417:337-370.
- 680 - Fedorov A.V., Dekens P.S., McCarthy M., Ravelo A.C., DeMenocal P.B., Barreiro, M.,
681 Pacanowski R.C., Philander S.G., (2006). The Pliocene paradox (mechanisms for a permanent El
682 Niño). *Science*, 312(5779), 1485-1489.
- 683 - Finocchiaro F., Langone L., Colizza E., Fontolan G., Giglio F., & Tuzzi E., (2005). Record of the
684 early Holocene warming in a laminated sediment core from Cape Hallett Bay (Northern Victoria
685 Land, Antarctica). *Global and Planetary Change*, 45(1-3), 193-206.
- 686 - Fox L.R., Wade B.S., Holbourn A., Leng M.J., Bhatia R., (2021). Temperature gradients across
687 the Pacific Ocean during the middle Miocene. *Paleoceanography and Paleoclimatology*,
688 e2020PA003924.
- 689 - Gariboldi K., Gioncada A., Bosio G., Malinverno E., Di Celma C., Tinelli C., Cantalamessa G.,
690 Landini W., Urbina M., Bianucci G., (2015). The dolomite nodules enclosing fossil marine
691 vertebrates in the East Pisco Basin, Peru: field and petrographic insights into the Lagerstätte
692 formation. *Palaeogeography, Palaeoclimatology, Palaeoecology*, 438, 81-95.
- 693 - Gariboldi K., Bosio G., Malinverno E., Gioncada A., Di Celma C., Villa I.M., Urbina M., Bianucci
694 G., (2017). Biostratigraphy, geochronology and sedimentation rates of the upper Miocene Pisco
695 Formation at two important marine vertebrate fossil-bearing sites of southern Peru. *Newsletters*
696 *on Stratigraphy*, 50(4), 417-444.
- 697 - Gariboldi K., Pike J., Malinverno E., Di Celma C., Gioncada A., Bianucci G., 2023. BSE images
698 of sample CLQ20, laminated diatomites, Upper Miocene Pisco Fm, Peru [Dataset]. Figshare,
699 <https://doi.org/10.6084/m9.figshare.22309204.v1>
- 700 - Gioncada A., Collareta A., Gariboldi K., Lambert O., Di Celma C., Bonaccorsi E., Urbina M.,
701 Bianucci G., (2016). Inside baleen: exceptional microstructure preservation in a late Miocene
702 whale skeleton from Peru. *Geology*, 44(10), 839-842.
- 703 - Gioncada A., Gariboldi K., Collareta A., Di Celma C., Bosio G., Malinverno E., Lambert O., Pike
704 J., Urbina M., Bianucci G., (2018a). Looking for the key to preservation of fossil marine
705 vertebrates in the Pisco Formation of Peru: new insights from a small dolphin skeleton. *Andean*
706 *Geology*, 45.3 (2018):379-398.
- 707 - Gioncada A., Petrini R., Bosio G., Gariboldi K., Collareta A., Malinverno E., Bonaccorsi E., Di
708 Celma C., Pasero M., Urbina M., Bianucci G., (2018b). Insights into the diagenetic environment
709 of fossil marine vertebrates of the Pisco Formation (late Miocene, Peru) from mineralogical and
710 Sr-isotope data. *Journal of South American Earth Sciences*, 81, 141-152.

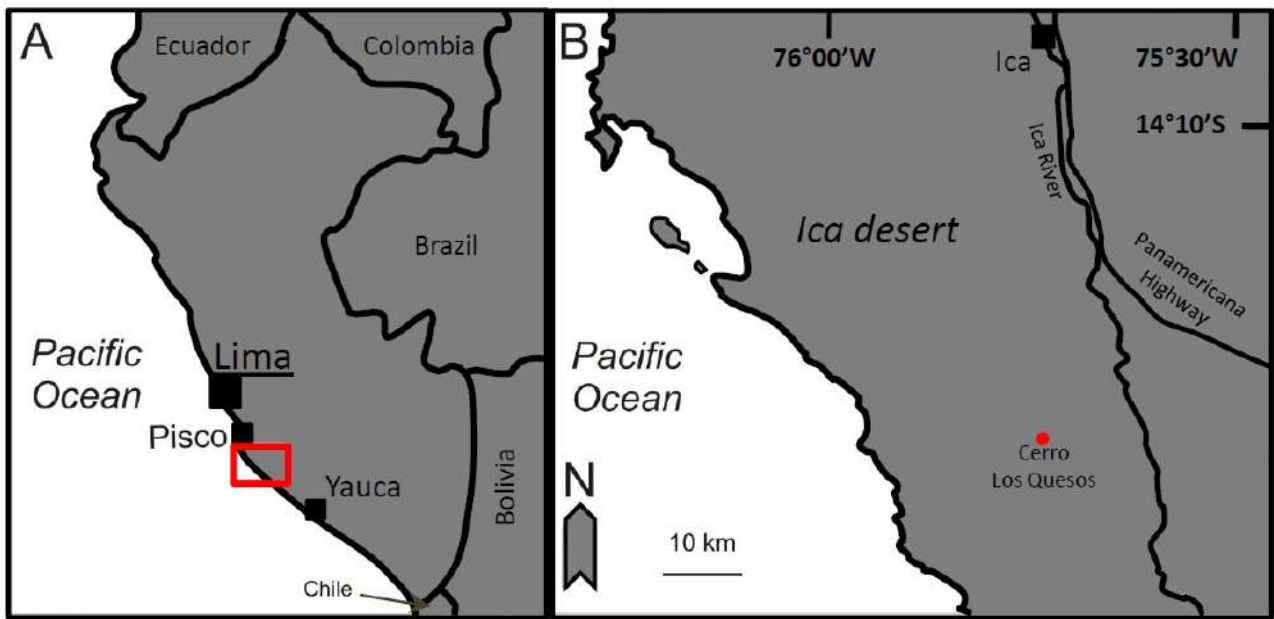
- 711 - Grigorov I., Pearce R.B., Kemp A.E.S., (2002). Southern Ocean laminated diatom ooze: mat
712 deposits and potential for palaeo-flux studies, ODP leg 177, Site 1093. *Deep-Sea Research*, 49,
713 3391-3407.
- 714 - Grimm K.A., Lange C.B., Gill A.S., (1996). Biological forcing of hemipelagic sedimentary
715 laminae; evidence from ODP Site 893, Santa Barbara Basin, California. *Journal of Sedimentary*
716 *Research*, 66(3), 613-624.
- 717 - Hamilton E.L., (1976). Variations of density and porosity with depth in deep-sea
718 sediments. *Journal of Sedimentary Research*, 46(2), 280-300.
- 719 - Hasle G.R., Syvertsen E.E., Steidinger K.A., Tangen K., Thronsen J., & Heimdal B.R. (1997).
720 Identification of Marine Phytoplankton.
- 721 - Hebbeln D., Marchant M., & Wefer, G. (2000). Seasonal variations of the particle flux in the Peru-
722 Chile current at 30 S under 'normal' and El Niño conditions. *Deep Sea Research Part II: Topical*
723 *Studies in Oceanography*, 47(9-11), 2101-2128.
- 724 - Herbert T.D., Lawrence K.T., Tzanova A., Peterson L.C., Caballero-Gill R., & Kelly C.S. (2016).
725 Late Miocene global cooling and the rise of modern ecosystems. *Nature Geoscience*, 9(11), 843-
726 847 (DOI: 10.1038/NCEO2813).
- 727 - Hill A.E., Hickey B.M., Shillington F.A., Strub P.T., Brink K.H., Barton E.D., and Thomas A.C.,
728 (1998), Eastern Ocean boundaries. In *The Sea*, vol. 11, edited by A. R. Robinson and K. H.
729 Brink, pp. 29– 67, John Wiley and Sons Edition, NY.
- 730 - Holbourn A., Kuhnt W., Lyle M., Schneider L., Romero O., Andersen, N., (2014). Middle
731 Miocene climate cooling linked to intensification of eastern equatorial Pacific
732 upwelling. *Geology*, 42(1), 19-22.
- 733 - Hsu J.T., 1992. Quaternary uplift of the Peruvian Coast related to the subduction of the Nazca
734 Ridge: 13.5 to 15.6 degrees south latitude. *Quaternary International*, 15–16, 87–97.
- 735 - Huyer A., Smith R.L., Paluszkiwicz T., (1987). Coastal upwelling off Peru during normal and El
736 Niño times, 1981–1984. *Journal of Geophysical Research: Oceans*, 92(C13), 14297-14307.
- 737 - Isaacs C.M., Pisciotto K.A., Garrison R.E., (1983). Facies and diagenesis of the Miocene
738 Monterey Formation, California: a summary. *Developments in Sedimentology*, 36: 247-282.
- 739 - Kemp A.E.S., (1990). Sedimentary fabrics and variation in lamination style in Peru continental
740 margin upwelling sediments. *Proceedings of ODP, Scientific Results*, 112, 43-58.
- 741 - Kemp A.E.S., Pearce R.B., Koizumi I., Pike J., Rance S.J., (1999). The role of mat-forming
742 diatoms in formation of the Mediterranean sapropels. *Nature*, 398, 57-61.
- 743 - Kemp A.E.S., Pike J., Pearce R.B., Lange C.B., (2000). The “Fall dump”-a new perspective on the
744 role of a “shade flora” in the annual cycle of diatom production and export flux. *Deep-Sea*
745 *Research II*, 47: 2129-2154.
- 746 - Lambert O., Bianucci G., Post K., de Muizon C., Salas-Gismondi R., Urbina M., Reumer J.,
747 (2010). The giant bite of a new raptorial sperm whale from the Miocene epoch of
748 Peru. *Nature*, 466(7302), 105.
- 749 - Lamy, F., Hebbeln, D., Röhl, U., & Wefer, G., (2001). Holocene rainfall variability in southern
750 Chile: a marine record of latitudinal shifts of the Southern Westerlies. *Earth and Planetary*
751 *Science Letters*, 185(3-4), 369-382.
- 752 - Liu Z., & Herbert T.D. (2004). High-latitude influence on the eastern equatorial Pacific climate in
753 the early Pleistocene epoch. *Nature*, 427(6976), 720-723.
- 754 - Maddison E.J., Pike J., Dunbar R., (2012). Seasonally laminated diatom-rich sediments from
755 Dumont d'Urville trough, East Antarctic margin: Late-holocene neoglacial sea-ice
756 conditions. *The Holocene*, 22(8), 857-875.
- 757 - Malinverno E., Bosio G., Gioncada A., Cimò R., Andò S., Mariani L., Coletti G., Boschi C.,
758 Gariboldi K., Galimberti L., Bianucci G., Urbina M., Di Celma C., (2023). Laterally-continuous
759 dolomite layers of the Miocene Pisco Formation (East Pisco Basin, Peru): a window into past
760 cyclical changes of the diagenetic environment. *Marine and Petroleum Geology*, 147, 105977.

- 761 - Marty R., (1988). Stratigraphy and chemical sedimentology of Cenozoic biogenic sediments from
762 the Pisco and Sechura Basins, Peru. PhD Thesis, Huston, Texas, Rice University.
- 763 - Marx, F.G., Uhen, M.D., (2010). Climate, critters, and cetaceans: Cenozoic drivers of the
764 evolution of modern whales. *Science*, 327(5968), 993-996.
- 765 - Meehl G.A., & Washington W.M. (1996). El Niño-like climate change in a model with increased
766 atmospheric CO₂ concentrations. *Nature*, 382, 56-60.
- 767 - Molina R.E., Manrique, F.A., García J., (1997). Nota sobre un florecimiento de *Stephanopyxis*
768 *palmeriana* (Greville) Grunow (Bacillariophyceae) en la bahía Kun Kaak, Golfo de
769 California. *Hidrobiológica*, 7(1), 84-86.
- 770 - Montoya M., García W., & Vidal J.C., (1994). Geología de los cuadrángulos de Lomitas, Palpa,
771 Nasca y Puquío: hojas 30-l, 30-m, 30-n, 30-ñ. Instituto Geológico Minero y Metalúrgico.
- 772 - Müller P. J., Kirst G., Ruhland G., Von Storch I., & Rosell-Melé A. (1998). Calibration of the
773 alkenone paleotemperature index U37K' based on core-tops from the eastern South Atlantic and
774 the global ocean (60 N-60 S). *Geochimica et cosmochimica Acta*, 62(10), 1757-1772.
- 775 - Navarro J.N. (1982). A survey of the marine diatoms of Puerto Rico. IV. Suborder Araphidineae:
776 Families Diatomaceae and Protoraphidaceae. *Botanica Marina*, Vol. XXIV.
- 777 Palmer A.A., Austin J.A. Jr., Schlager W., (1986). Introduction and explanatory notes. *Proceedings*
778 *of ODP, Scientific Results*, 101, 5-23.
- 779 - Pike J., Kemp A.E.S., (1996a). Preparation and analysis techniques for studies of laminated
780 sediments. In: *Palaeoclimatology and Palaeoceanography from laminated sediments*, ed. by
781 A.E.S. Kemp, No°116: 37-48. Geological Society Special Publication, London.
- 782 - Pike J., Kemp A.E.S., (1996b). Records of seasonal flux in Holocene laminated sediments, Gulf of
783 California. In: *Palaeoclimatology and Palaeoceanography from laminated sediments*, ed. by
784 A.E.S. Kemp, No°116: 157-170. Geological Society Special Publication, London.
- 785 - Pike J., Kemp A.E.S., (1997). Early Holocene decadal-scale ocean variability recorded in Gulf of
786 California laminated sediments. *Paleoceanography*, 12(2): 227-238.
- 787 - Pike J., Kemp A.E.S., (1999). Diatom mats in Gulf of California sediments: Implication for the
788 paleoenvironmental interpretation of laminated sediments and silica burial. *Geology*, 27(4): 311-
789 314.
- 790 - Pike J., Bernhard J.M., Moreton S.G., Butler I.B., (2001). Microbioirrigation of marine sediments
791 in dysoxic environments: implications for early sediment fabric and diagenetic processes.
792 *Geology*, 29 (10): 923-926.
- 793 - Pike J., Stickley C.E., (2013). Diatom fossil record from marine laminated sediments. In:
794 *Encyclopedia of Quaternary Science*, ed. By S. Elias, C. Mock, Vol. 1: 554-561.
- 795 - Pilskalns C.H., Pike J. (2001). Formation of Holocene sedimentary laminae in the Black Sea and
796 the role of the benthic flocculent layer. *Paleoceanography*, 16, 1-19.
- 797 - Ragaini L., Di Celma C., Cantalamessa G., (2008). Warm-water mollusc assemblages from
798 northern Chile (Mejillones Peninsula): new evidence for permanent El Niño-like conditions
799 during Pliocene warmth? *Journal of the Geological Society*, London, 165, 1075-1084.
- 800 - Ravelo A.C., Deken P. S., McCarthy M., (2006). Evidence for El Niño-like conditions during the
801 Pliocene. *Gsa Today*, 16(3), 4.
- 802 - Ravelo A.C., Lawrence K.T., Fedorov A., Ford H.L., (2014). Comment on “A 12-million-year
803 temperature history of the tropical Pacific Ocean”. *Science*, 346(6216), 1467.
- 804 - Rea, D. K., Basov, I. A., Janecek, T. R., Palmer-Julson, A. et al., (1993). *Proceedings of the*
805 *Ocean Drilling Program, Initial Reports*, 145, 9-33.
- 806 - Romero O., Hebbeln D., (2003). Biogenic silica and diatom thanatocoenosis in surface sediments
807 below the Peru-Chile Current: controlling mechanisms and relationship with productivity of
808 surface waters. *Marine Micropaleontology*, 48(1-2), 71-90.
- 809 - Romero O., Lange C., & Hebbeln, D. (2002). Effects of El Niño 1997-98 on Particle Fluxes from
810 two Coastal Upwelling Areas: Northern Chile and Southern California. *Investigaciones*
811 *marinas*, 30(1), 172-173.

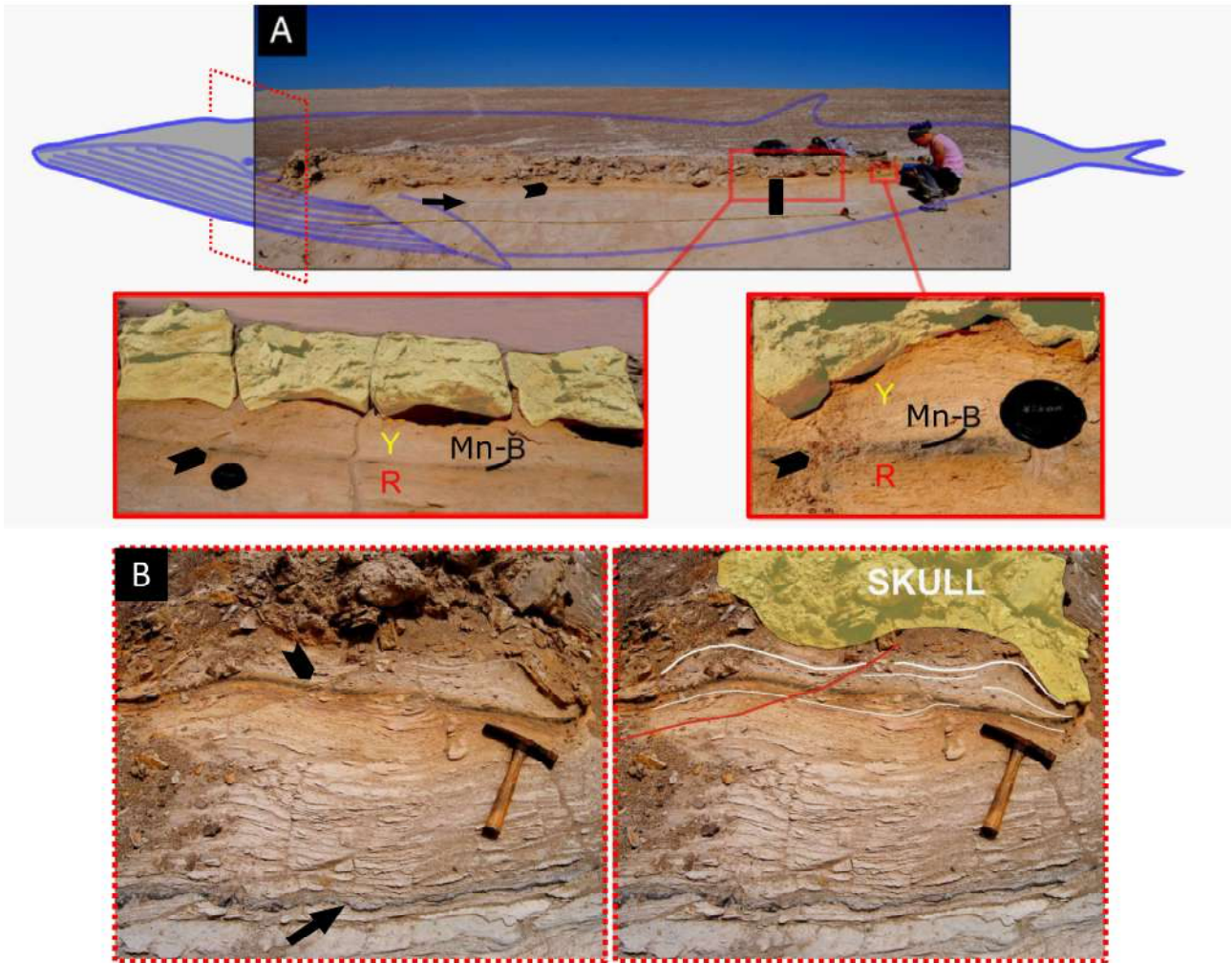
- 812 - Round F.E., Crawford R.M., & Mann, D.G., (1990). Diatoms: biology and morphology of the
813 genera. Cambridge University Press.
- 814 - Rousselle G., Beltran C., Sicre M.A., Raffi I., De Rafelis M., (2013). Changes in sea-surface
815 conditions in the Equatorial Pacific during the middle Miocene–Pliocene as inferred from
816 coccolith geochemistry. *Earth and planetary science letters*, 361, 412-421
817 (<http://dx.doi.org/10.1016/j.epsl.2012.11.003>).
- 818 - Sancetta C., (1995). Diatoms in the Gulf of California: seasonal flux patterns and the sediment
819 record for the last 15,000 years. *Paleoceanography*, 10 (1): 67-84.
- 820 - Seki O., Schmidt D.N., Schouten S., Hopmans E.C., Sinninghe Damsté J.S., & Pancost R.D.
821 (2012). Paleoceanographic changes in the Eastern Equatorial Pacific over the last 10
822 Myr. *Paleoceanography*, 27(3).
- 823 - Schuette G., & Schrader H. (1981). Diatom taphocoenoses in the coastal upwelling area off South
824 West Africa. *Marine Micropaleontology*, 6(2), 131-155.t
- 825 - Schuette G., & Schrader H. (1981b). Diatoms in surface sediments: a reflection of coastal
826 upwelling. *Coastal upwelling*, 1, 372-380.
- 827 - Schrader H., (1982). Diatom biostratigraphy and laminated diatomaceous sediments from the Gulf
828 of California Deep Sea Drilling Project Leg 64. In Curray, J.R., More, D.G., Kelts, K., Einsele,
829 G. *Proceedings of the Ocean Drilling Program, Part A: Initial Reports* 64(2), p. 1089-1116.
- 830 - Schrader H.J., Gersonde R., (1978). Diatoms and silicoflagellates. In: Zachariasse A., Riedel
831 W.R., Sanfilippo A., Schmidt R.R., Broelsma M.J., Schrader H.J., Gersonde R., Drooger
832 M.M., Broekman J.A. (Editors), *Micropaleontological counting methods and techniques — An*
833 *exercise on an eight meters section of the Lower Pliocene of Capo Rossello, Sicily. Utrecht*
834 *Micropaleontology Bulletin*, 17, 129–176
- 835 - Shankle M.G., Burls N.J., Fedorov A.V., Thomas M.D., Liu W., Penman D.E., Ford H.L., Jacobs
836 P.H., Planavsky N., & Hull, P. M. (2021). Pliocene decoupling of equatorial Pacific temperature
837 and pH gradients. *Nature*, 598(7881), 457-461.
- 838 - Shipe R.F., Passow U., Brzezinski M.A., Graham W.M., Pak D.K., Siegel D.A., & Alldredge A.
839 L. (2002). Effects of the 1997–98 El Niño on seasonal variations in suspended and sinking
840 particles in the Santa Barbara basin. *Progress in Oceanography*, 54(1-4), 105-127.
- 841 - Suess E., von Huene R. et al., (1988). *Proceeding of the Ocean Drilling Program, Initial Reports*
842 *112*. College Station, TX (Ocean Drilling Program).
- 843 - Sournia A., (1982). Is there a shade flora in the marine plankton? *Journal of Phytoplankton*
844 *Research*, 4: 391-399.
- 845 - Stickley C.E., Pike J., Leventer A., Dunbar R., Domack E.W., Brachfeld S., Manley P.,
846 McClennan C., (2005). Deglacial ocean and climate seasonality in laminated diatom sediments,
847 Mac. Robertson Shelf, Antarctica. *Palaeogeography, Palaeoclimatology, Palaeoecology*, 227(4),
848 290-310.
- 849 - Strub P.T., Mesías J.M., Montecino V., Rutllant J., Salinas S., (1998). Coastal Ocean Circulation
850 off Western South America, Coastal Segment. In: Robinson, A.R., Brink, K.H. (Editors), *The*
851 *Sea*, Volume 11. The Global Coastal Ocean, Regional Studies and Synthesis. Wiley, New York,
852 pp. 273-313.
- 853 - Tesi T., Belt S.T., Gariboldi K., Muschitiello F., Smik L., Finocchiaro F., Giglio F., Colizza E.,
854 Gazzurra G., Giordano P., Morigi C., Capotondi L., Nogarotto A., Köseoğlu D., Di Roberto A.,
855 Gallerani, A., Langone, L., (2020). Resolving sea ice dynamics in the north-western Ross Sea
856 during the last 2.6 ka: From seasonal to millennial timescales. *Quaternary Science Reviews*, 237,
857 106299.
- 858 - Thornburg T.M., Kulm L.D., (1981). Sedimentary basins of the Peru continental margin: structure,
859 stratigraphy, and Cenozoic tectonics from 6°S to 16° latitude. In: Kulm, L.D., Dymond, J.,
860 Dasch, E.J., Hussong, D.M. (Eds.), *Nazca Plate: Crustal Formation and Andean Convergence*.
861 Geological Society of America, Memoir 154, pp. 393–422.

- 862 - Thunell R., Pride C., Tappa E., Muller-Karger F., (1993). Varve formation in the Gulf of
 863 California: insights from time series sediment trap sampling and remote sensing. *Quaternary*
 864 *Science Reviews*, 12: 451-464.
- 865 - Wara M.W., Ravelo A.C., Delaney M.L., (2005). Permanent El Niño-like conditions during the
 866 Pliocene warm period. *Science*, 309(5735), 758-761.
- 867 - Wefer G., Berger W.H., Richter C., (1998). The Angola-Benguela upwelling system:
 868 paleoceanography synthesis of shipboard results from LEG 1751. In *Proceeding of the Ocean*
 869 *Drilling Program*, Initial Reports. 175. Texas A&M University, College Station, Texas.
- 870 - White S.M., Ravelo A.C., (2020a). Dampened El Niño in the early Pliocene warm
 871 period. *Geophysical Research Letters*, 47(4), e2019GL085504.
- 872 - White S.M., Ravelo A.C., (2020b). The benthic B/Ca record at Site 806: new constraints on the
 873 temperature of the West Pacific Warm Pool and the “El Padre” state in the
 874 Pliocene. *Paleoceanography and Paleoclimatology*, 35(10), e2019PA003812.
- 875 - Zhang Y.G., Pagani M., Liu Z., (2014a). A 12-million-year temperature history of the tropical
 876 Pacific Ocean. *Science*, 344(6179), 84-87.
- 877 - Zhang Y.G., Pagani M., Liu Z., (2014b). Response to Comment on “A 12-million-year
 878 temperature history of the tropical Pacific Ocean”. *Science*, 346(6216), 1467-1467.

879
 880 FIGURES

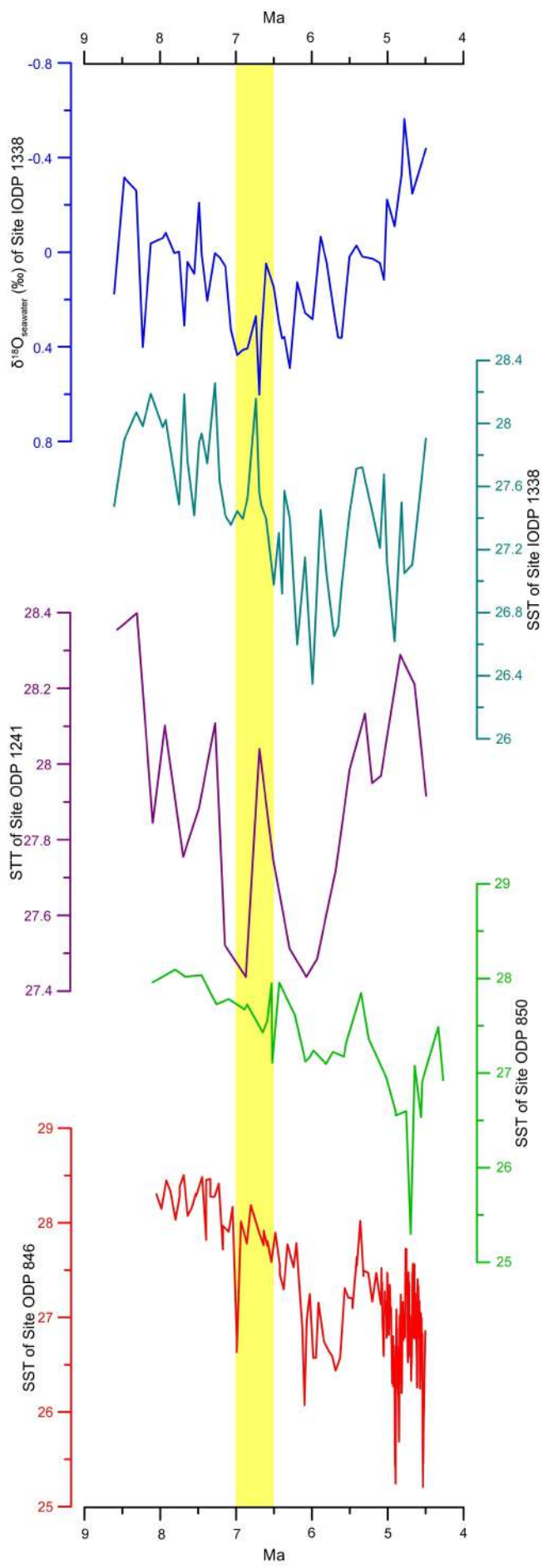


881
 882 Figure 1. Geographic setting of the Ica desert. A. Sketch map of Peru, with location of the Ica desert
 883 (red square). B. Close up of the Ica desert; location of Cerro Los Quesos (CLQ).

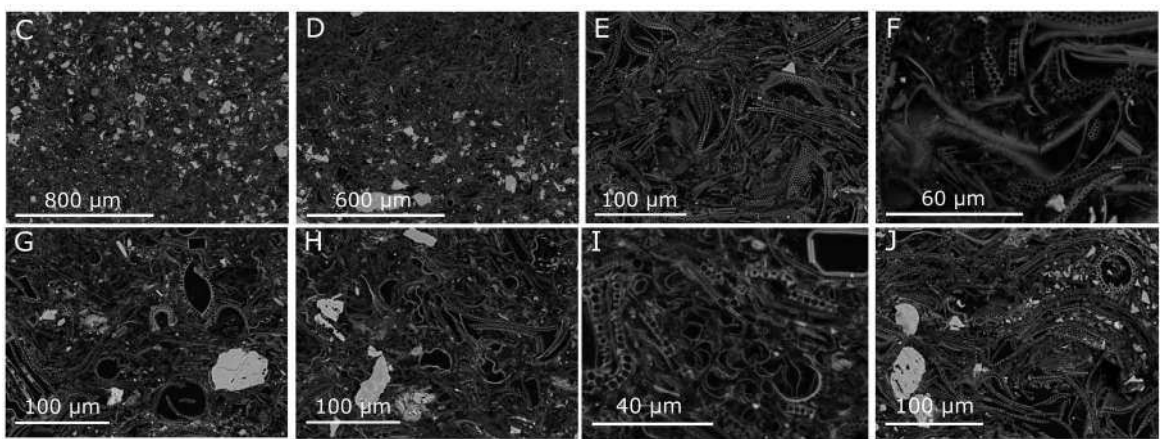
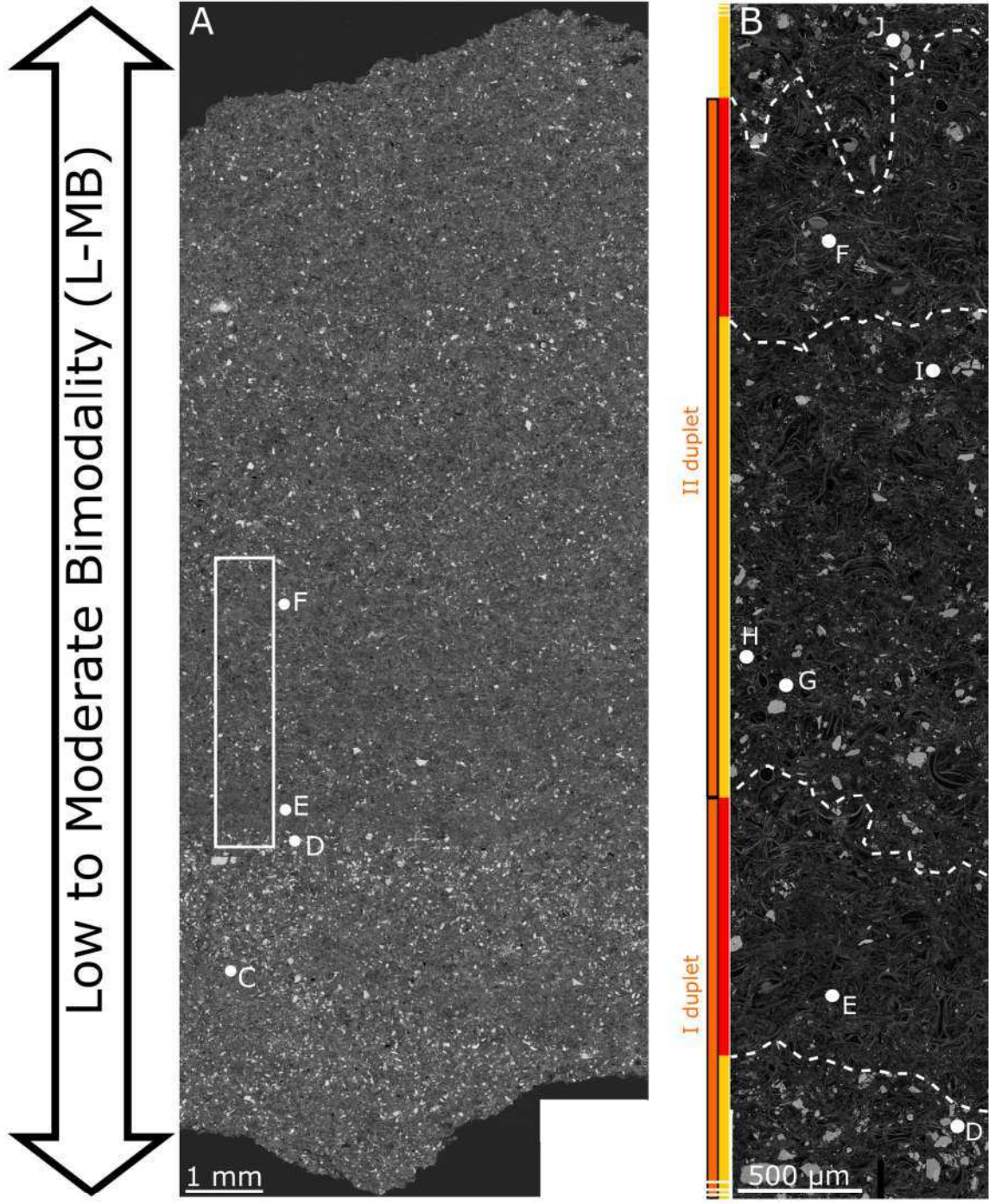


884

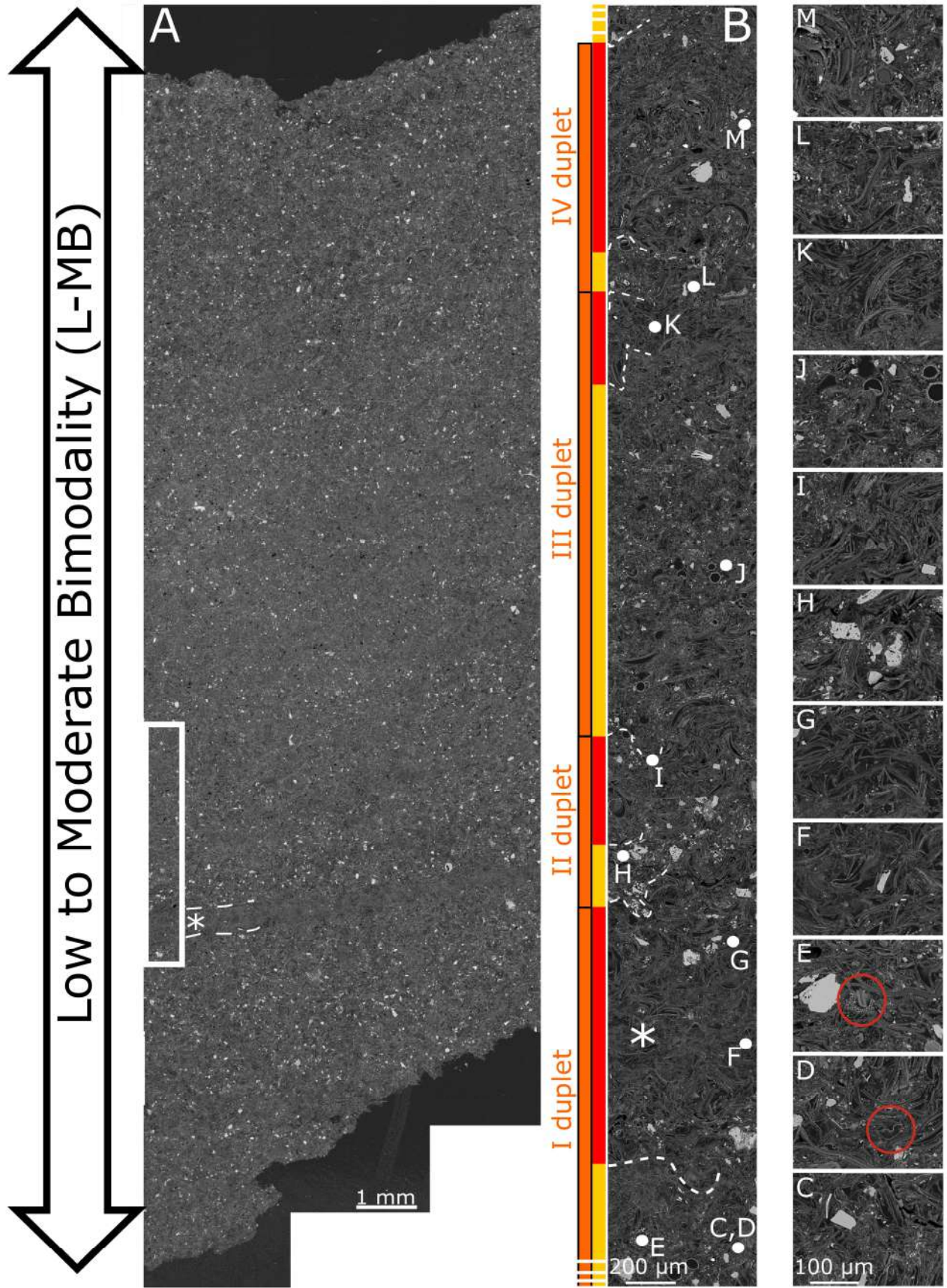
885 Figure 2. Fossil whale CLQ M58 (14°30'58.3"S; 75°43'04.5"W) at Cerro Los Quesos, Ica Desert,
 886 Peru. A. CLQ M58 in the outcrop. Black rectangle: location of the CLQ20 sample; black arrow:
 887 black tephra underneath CLQ M58 (not dated); black arrowhead: Mn layer of the YBR sequence
 888 (see text for explanation). The two red rectangles show the yellow portion of diatomites ("Y")
 889 underlain by a black manganese-rich layer ("Mn-B") and by reddish diatomites ("R") related to
 890 geochemical processes activated by the decomposition of the carcass (see Gariboldi et al., 2015;
 891 Gioncada et al., 2018). Camera dust cap for scale. The red dotted square highlights the position of
 892 Fig. 2B in respect to M58. 2B. Detailed of the diatomites below the skull of M58; right: the
 893 sedimentary features observed in the left picture are outlined. Laminations (white lines) are
 894 deformed by the weight of the skull (yellow area) and in some points cut by the Mn layer (black
 895 arrowhead in the left picture). These deformations highlight that the carcass sank into the soupy,
 896 plastic diatomitic sediments as it reached the seabed. The geometry of the Mn layer with respect to
 897 the laminations shows that it precipitated after the diatomites were deformed. Red continuous line
 898 highlights secondary deformations. The black arrow points to the black tephra layer. Hammer as a
 899 scale. Modified from Gariboldi et al., 2015 and Bosio et al., 2021b.



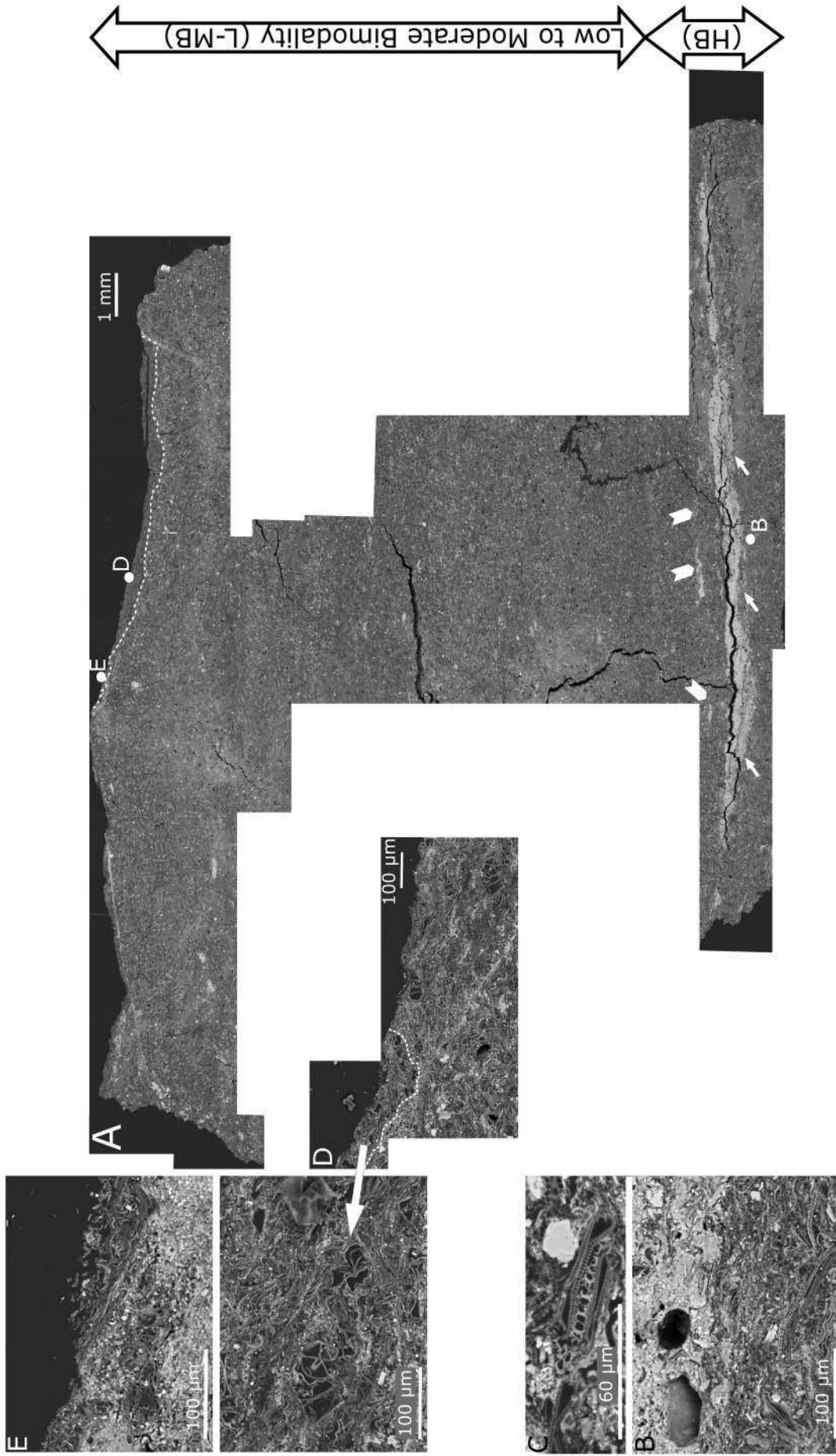
901 Figure 3. Temporal context of the CLQ20 sample and $\delta^{18}\text{O}$ and SST values for the Eastern
902 Equatorial Pacific in the 9-4 Ma range. Sample CLQ20 was deposited between an older age limit of
903 6.93 ± 0.09 Ma, and a younger lower limit of $\geq 6.71 \pm 0.02$ Ma (yellow rectangle; Messinian), as
904 suggested by two dated tephra in the CLQ stratigraphic succession; a) the $\delta^{18}\text{O}_{\text{seawater}}$ (‰) for IODP
905 Site 1338 (Rousselle et al., 2013) and SST ($^{\circ}\text{C}$) values for: b) IODP Site 1338 (Rousselle et al.,
906 2013); c) ODP Site 1241 (Seki et al., 2012); d) ODP Site 850 (Zhang et al., 2014); e) ODP Site 846
907 (Liu and Herbert, 2004). The CLQ20 sample dates back to a period characterised by high values of
908 $\delta^{18}\text{O}_{\text{seawater}}$ and SST as high as during the Middle Pliocene Warm Period (see fig. 5 of Rousselle et
909 al., 2013). All SST shown are calculated following the U^{k}_{37} calibration proposed by Müller et al.,
910 1998.
911
912



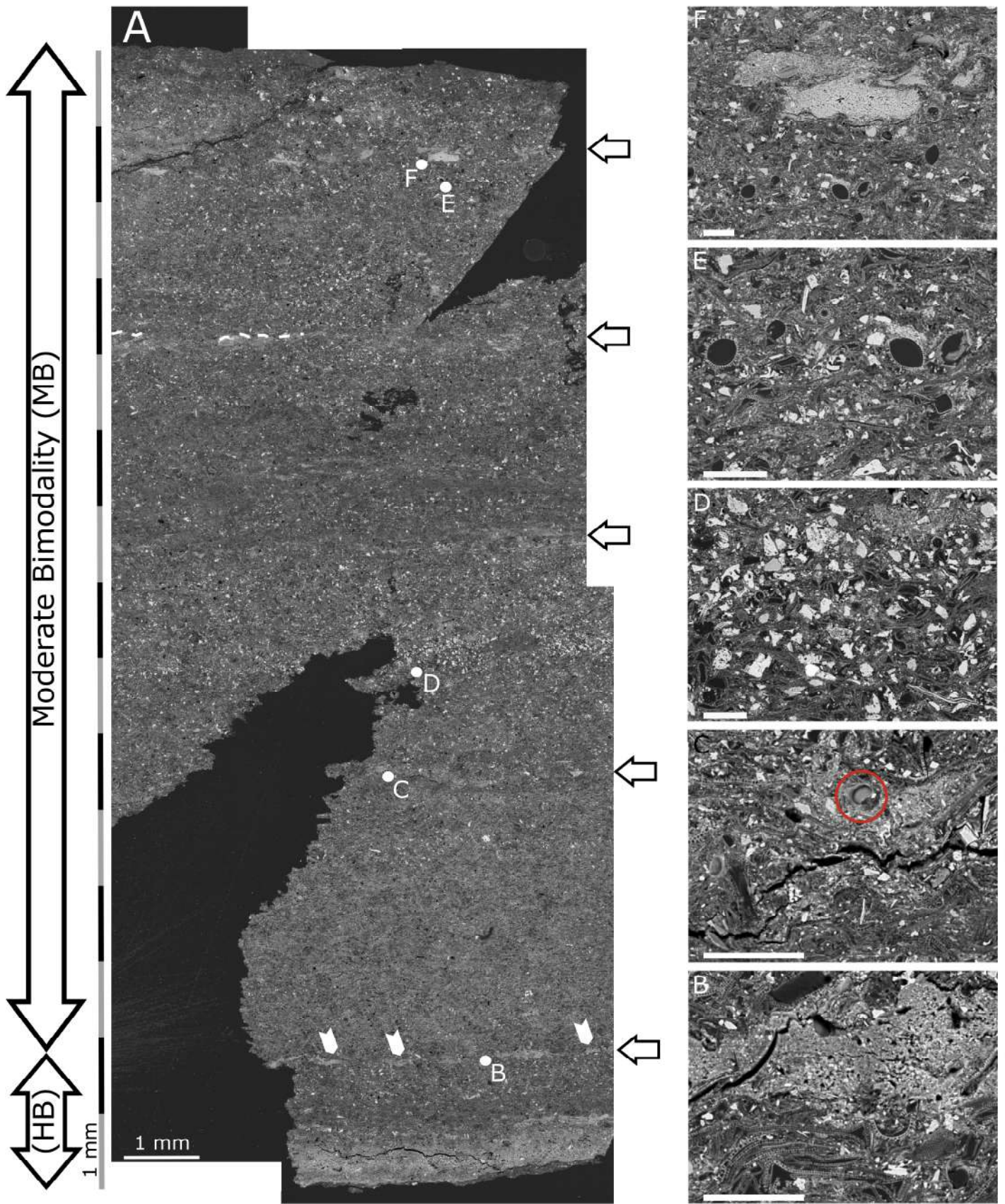
914 Figure 4. BSE-SEM images of slide t13. A. Low magnification (100x) BSE image of slide t13,
915 which is characterised by a low to moderate bimodality (L-MB). This bimodality pattern is mostly
916 given by the sparse presence of silt particles within a darker matrix (diatomite). The white rectangle
917 indicates the position of 4B; letters highlight the same spots in 4A and 4B as well as in Figs 4C-4J.
918 The mixed lamina (yellow rectangles) - *Coscinodiscus lamina* (red rectangles) duplets (orange
919 rectangles) are discernible. Mixed laminae are particularly recognizable due to the presence of silt
920 particles. Boundaries between laminae (white dotted lines) are wavy and indistinct. Coloured
921 rectangles are dotted when laminae are not pictured in their whole length. C. Silt particles in mixed
922 lamina. D. Boundary between a mixed lamina (bottom) and a *Coscinodiscus* lamina (top). E. Detail
923 of *Coscinodiscus* frustules in a *Coscinodiscus* lamina. F. Detail of *Actinocyclus octonarius* frustules
924 in a *Coscinodiscus* lamina. G. Detailed of a mixed lamina; silt particles, *Stephanopyxis* frustules and
925 *Actinoptychus* cf. *senarius* frustules are visible. H. Detailed of *Actinoptychus* cf. *senarius* frustules
926 in a mixed lamina. I. A bunch of *Chaetoceros Hyalochaete* resting spores in a mixed lamina. J.
927 Detail of a mixed lamina: silt particles, *Coscinodiscus* frustules and *Stephanopyxis* frustules are
928 visible.



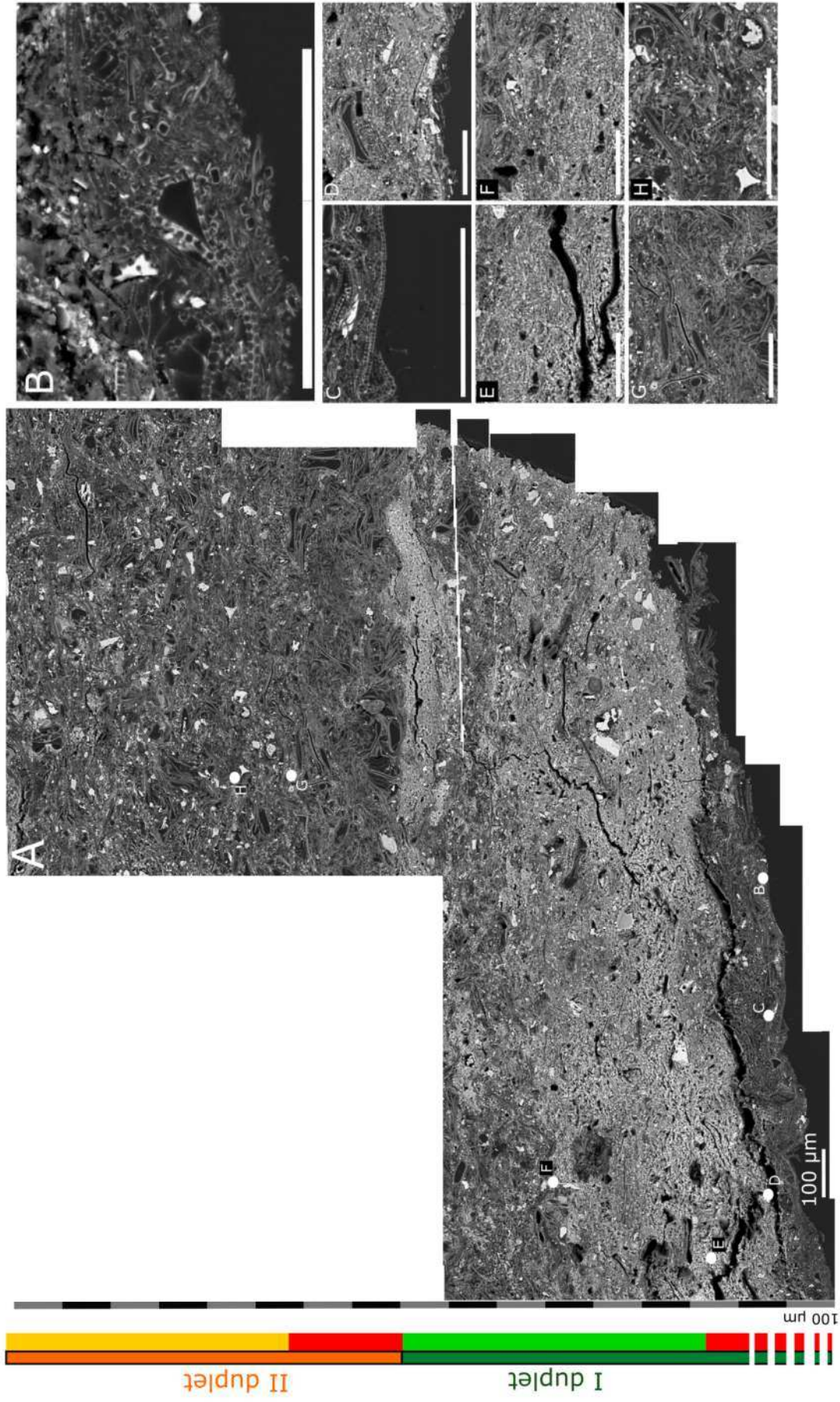
930 Figure 5. BSE-SEM images of slide t14. A. Low magnification (100x) BSE image of slide t14,
931 which is characterised by a low to moderate bimodality (L-MB). This bimodality pattern is mostly
932 given by the sparse presence of silt particles within a darker matrix (diatomites). The white
933 rectangle indicates the position of 5B, while the asterisk highlights the position of a *Coscinodiscus*
934 lamina particularly evident even at low magnification (this lamina is visible also in 5B and 5F;
935 dotted lines outlines part of the *Coscinodiscus* lamina boundaries, which are wavy, quite distinct
936 and continuous. B. 800x magnification of slide t14; four mixed lamina (yellow rectangles) -
937 *Coscinodiscus* lamina (red rectangles) duplets (orange rectangles) are discernible, but the lowest
938 one lacks the bottom of the mixed lamina. The sequence represented in 5B ends with the bottom of
939 a mixed lamina (yellow rectangle). Coloured rectangles are dotted when laminae are not pictured in
940 their whole length. The mixed lamina – *Coscinodiscus* lamina duplets have thickness varying from
941 625 μm to ca. 1750 μm , with a huge difference in the thickness of the two mixed laminae (ca. 375
942 μm in the second duplet vs. ca. 1500 μm in the third duplet). The *Coscinodiscus* lamina of the
943 second and third duplets have more similar thicknesses (ca. 250 μm) but the *Coscinodiscus* lamina
944 of the first and fourth duplets are ca. 1000 μm thick (thickness of laminae are approximate as their
945 thickness vary along their length). Letters highlights the position of images in the right column. C.
946 silt particles in a mixed lamina. D. *Actinopteryx* cf. *senarius* frustule in a mixed lamina (circled in
947 red). E. Silt particle and *Stephanopyxis* valve (circled in red) in a mixed lamina. F, G.
948 *Coscinodiscus* frustules and silt particle in a *Coscinodiscus* lamina. H. Silt particles and
949 *Coscinodiscus* frustules in a mixed lamina. I. *Coscinodiscus* lamina at its upper boundary with a
950 mixed lamina. J. *Stephanopyxis* frustules and silt particles in a mixed lamina. K. *Coscinodiscus*
951 frustules in a *Coscinodiscus* lamina. L. Silt particles and *Coscinodiscus* frustules in a mixed lamina.
952 M. *Coscinodiscus* frustules and silt particle in a *Coscinodiscus* lamina. The 100 μm scale bar is
953 valid for figures 5C-M.



955 Fig 6. BSE-SEM images of slide t5. A. Low magnification (100x) BSE image of slide t5,
956 characterised at its bottom by a high bimodality, given by the contrast of a terrigenous lamina and
957 the terrigenous boudinage-like top of a mixed lamina (arrowheads) with the underlying and
958 overlying biogenic laminae. The rest of the slide is characterised by a low to moderate bimodality
959 (L-MB). This bimodality pattern is mostly given by the sparse presence of silt particles within a
960 darker matrix (diatomite). White arrows at the bottom point to the lower boundary of the
961 terrigenous lamina, which is straight to wavy but sharp. The dotted line at the top of the image
962 highlights a wavy boundary between a terrigenous lamina and the overlying *Actinoptychus* cf.
963 *senarius* lamina. Letters highlight the position of images in the left column. B. Detail of the lower
964 boundary of the terrigenous lamina (the content of the underlying lamina is not defined, due to the
965 imperfect polishing of the slide). C. *Thalassionema* specimens in the terrigenous lamina. D, E.
966 Details of the boundary between the terrigenous lamina and the overlying *Actinoptychus* cf.
967 *senarius* lamina; the white arrow in D points to an enlarged image of the *Actinoptychus* cf.
968 *senarius* frustules.
969



972 Fig. 7. BSE-SEM images of slide t9. A. Low magnification (100x) BSE image of slide t9, which is
973 characterised at its bottom by a high bimodality, given by the contrast of a terrigenous lamina and
974 the terrigenous boudinage-like top of a mixed lamina (arrowheads) with the overlying biogenic
975 laminae (see Figs. 7B; 8A). The rest of the slide is characterised by moderate bimodality (MB)
976 given by the sparse presence of silt particles in mixed laminae, which alternates with *Coscinodiscus*
977 laminae (see Fig. S2) within a darker matrix (diatomite). White arrows indicate the thin terrigenous
978 boudinage-like top of the mixed laminae. The dotted line represents a continuous, straight but faint,
979 upper boundary between the terrigenous top of a mixed lamina with a *Coscinodiscus* lamina. Letters
980 highlights the position of images in the right column. B. Lower boundary of the terrigenous top of a
981 mixed lamina. C. Detail of a diatom valve (red circle) within the terrigenous top of the mixed
982 lamina. D. Silt particles in a mixed lamina. E. *Stephanopyxis* frustules within a mixed lamina. F.
983 Boudinage-like structure of the terrigenous top of a mixed lamina. Scale bars in 7B-F: 100 μm .
984



988 Figure 8. BSE-SEM images of slide t9. A. High magnification (2000x) BSE image of the bottom of
 989 slide t9 (the same visible in Fig. 7A). Letters highlights the position of images in Figs 8B-8H. B.
 990 Details of *Thalassionema* specimens within a *Coscinodiscus* lamina. C. Silt particle within a
 991 *Coscinodiscus* lamina. D. Detail of sparse diatom frustules within a terrigenous lamina. E. Detail of
 992 a terrigenous lamina. F. Boundary between a terrigenous lamina with the overlying *Coscinodiscus*
 993 lamina. The boundary is wavy and interdigitated. G. Boundary between a *Coscinodiscus* lamina
 994 with the overlying mixed lamina. The boundary is wavy, and faint, but continuous. H. *Chaetoceros*
 995 *Hyalochaete* resting spores within a mixed lamina. Scale bars in 8B-H: 100 µm.

996
 997 TABLE

998 Table 1. Ecology of principal diatom genera and species listed in this paper.

Genus/Species	Ecology
<i>Actinocyclus octonarius</i> Ehrenberg, 1837	Meroplanktic species correlated with the distribution of <i>Coscinodiscus</i> (Schuette and Schrader, 1981b).
<i>Actinoptychus senarius</i> (Ehrenberg) Ehrenberg 1843	Neritic (Cupp, 1943); typical of coastal upwelling assemblages (Abrantes et al., 2007).
<i>Chaetoceros</i> Ehrenberg, 1844 <i>Hyalochaete</i> Gran, 1897 spp. RS	A truly planktic genus. Most of <i>Chaetoceros</i> species are neritic, although some are oceanic. No fresh-water species are known (Cupp, 1943). <i>Chaetoceros</i> RS form at the end of upwelling bloom (spring and autumn), when the surface waters are depleted in nutrients (Schuette and Schrader, 1981a, b; Kemp et al., 2000; Romero and Hebbeln 2003).
<i>Coscinodiscus</i> Ehrenberg, 1839, nom. et typ. cons.	Recorded in modern environments as repeatedly forming continuous belts and patches (Schuette and Schrader, 1981b). Thrives at the thermo/nutricline at low light conditions, prefers a stratified water column (paart of the "shade flora") (Sournia, 1982; Kemp et al., 2000).
<i>Coscinodiscus asteromphalus</i> Ehrenberg, 1844	<i>C. asteromphalus</i> tolerates a wide range of temperatures and may be cosmopolitan (Hasle and Syvertsen, 1997).
<i>Stephanopyxis turris</i> (Greville) Ralfs 1861	Neritic, temperate and subtropical species (Cupp, 1943).
<i>Thalassionema</i> Grunow ex Mereschkowsky, 1902	A common marine plankton genus (Round, 1990).
<i>Thalassionema nitzschioides</i> (Grunow) Mereschkowsky, 1902	Marine, neritic and estuarine species; euryhaline and eurythermal (Navarro, 1982). It blooms in spring and summer (Schuette and Schrader, 1981a). <i>Thalassionema nitzschioides</i> var. <i>nitzschioides</i> is classified as part of the coastal upwelling group by Romero and Hebbeln, 2003.

999